

A Simple Model for the Evaporation of Hydrometers and Their Isotopes

Simon P. de Szoeke¹, Mampi Sarkar², Estefanía Quiñones Meléndez¹, Peter N. Blossey³, and David C Noone⁴

¹Oregon State University

²University of Houston

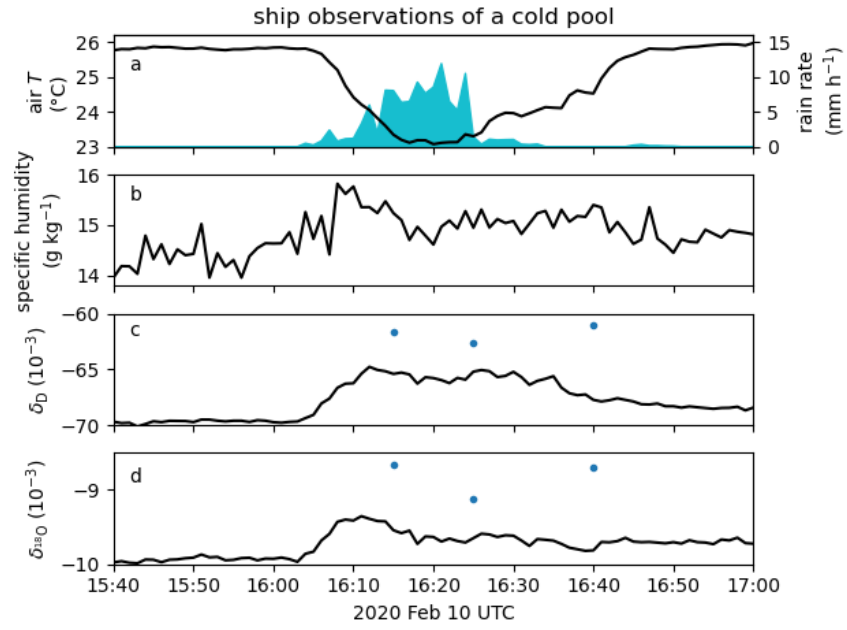
³University of Washington

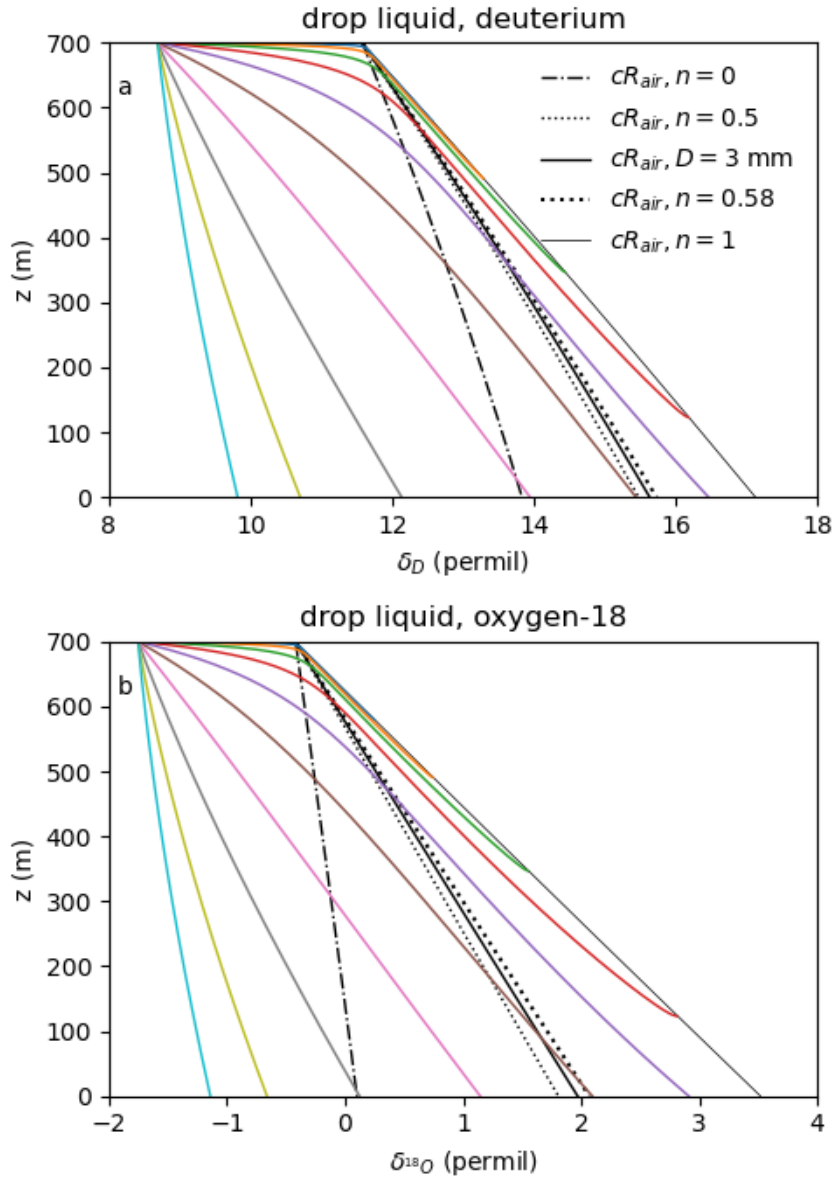
⁴University of Auckland

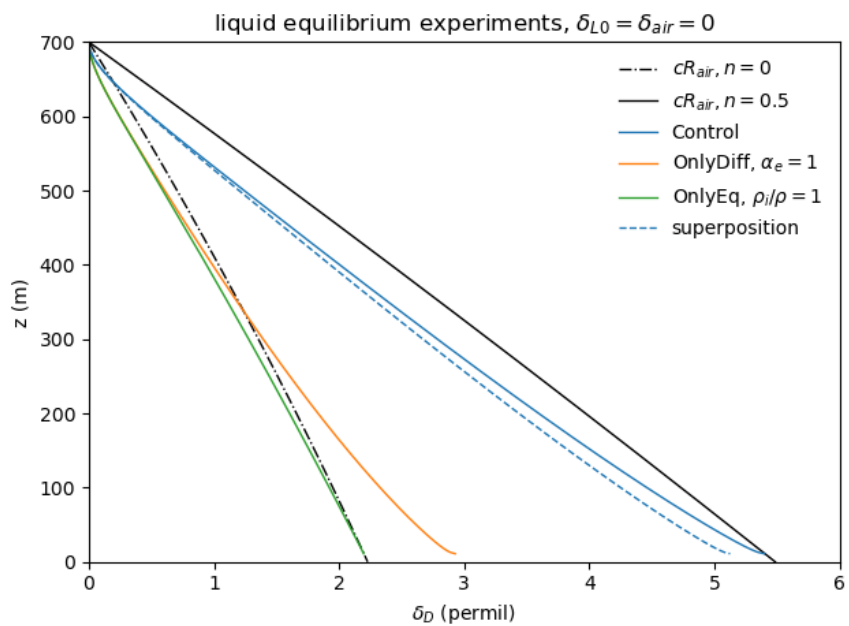
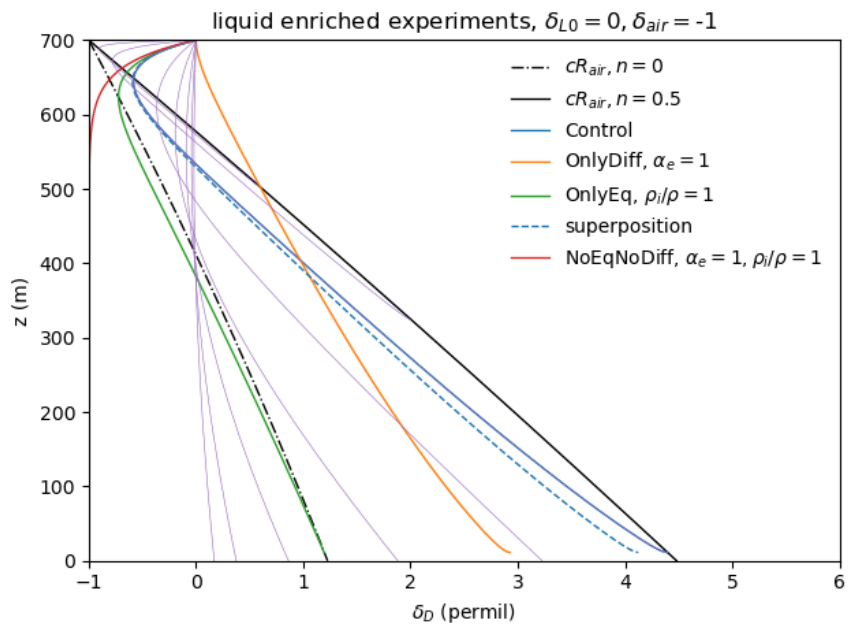
April 16, 2024

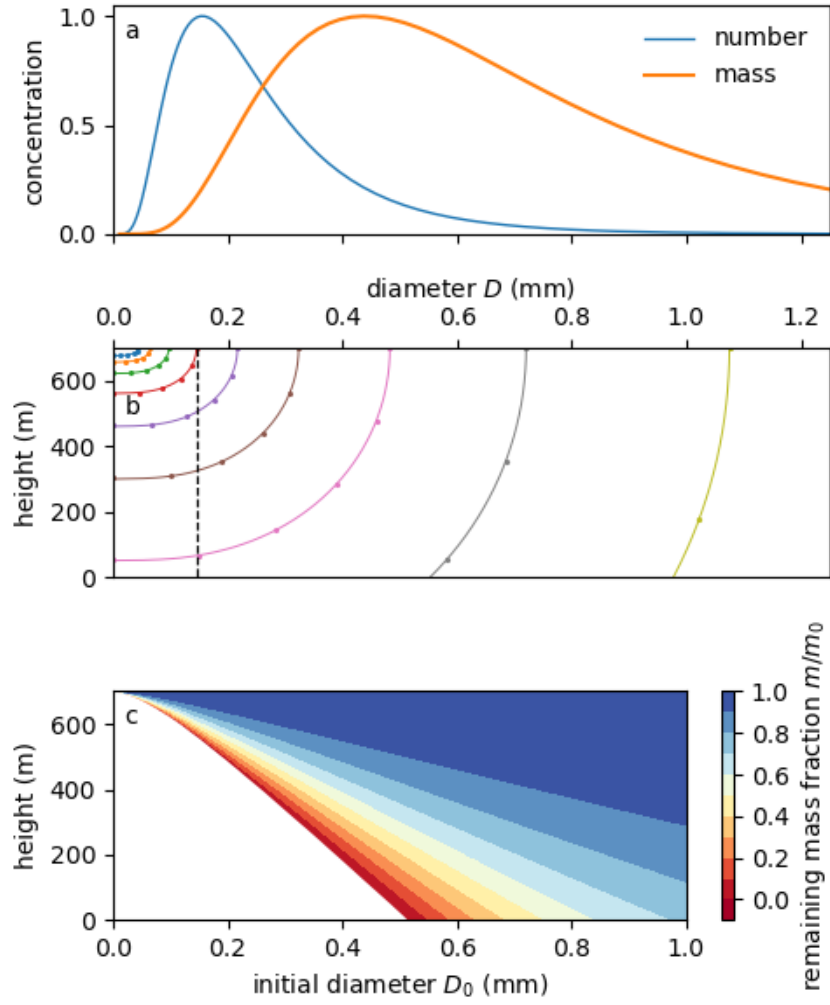
Abstract

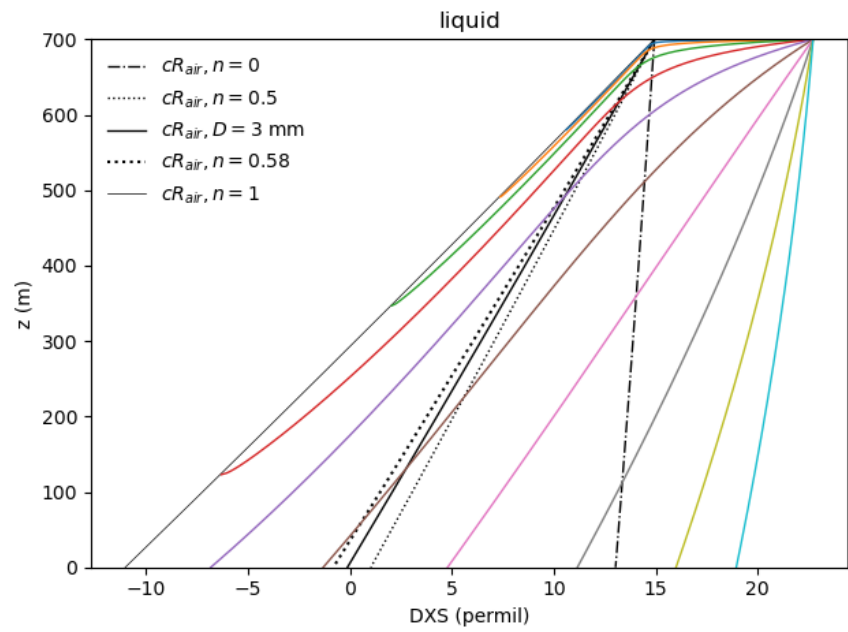
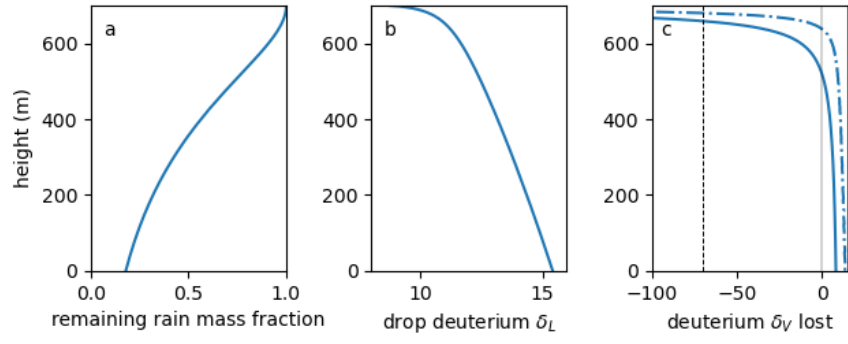
Evaporation decreases the mass and increases the isotope composition of falling drops. Combining and integrating the dependence of the evaporation on the drop diameter and on the drop-environment humidity difference, the square of drop diameter is found to decrease with the square of vertical distance below cloud base. Drops smaller than 0.5 mm evaporate completely before falling 700 m in typical subtropical marine boundary layer conditions. The effect on the isotope ratio of equilibration with the environment, evaporation, and kinetic molecular diffusion is modeled by molecular and eddy diffusive fluxes after Craig and Gordon (1965), with a size-dependent parameterization of diffusion that enriches small drops more strongly, and approaches the rough aerodynamic limit for large drops. Rain shortly approaches a steady state with the subcloud vapor by exchange with a length scale of 40 m. Kinetic molecular diffusion enriches drops up to as they evaporate by up to +5‰ for deuterated water (HDO) and +3.5‰ for H₂¹⁸O. Rain evaporation enriches undiluted subcloud vapor by +12‰ per mm rain, explaining enrichment of vapor in evaporatively cooled downdrafts that contribute to cold pools. Microphysics enriches the vapor lost by the early and complete evaporation of smaller drops in the distribution. Vapor from hydrometeors is more enriched than it would be by Rayleigh distillation or by mixtures of liquid rain and vapor in equilibrium with rain.

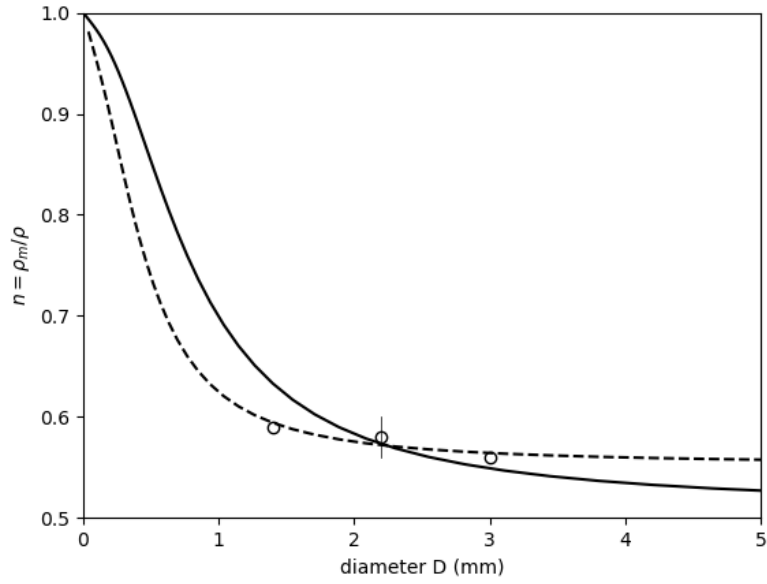
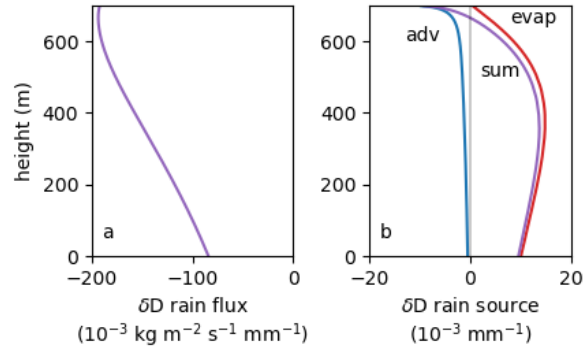


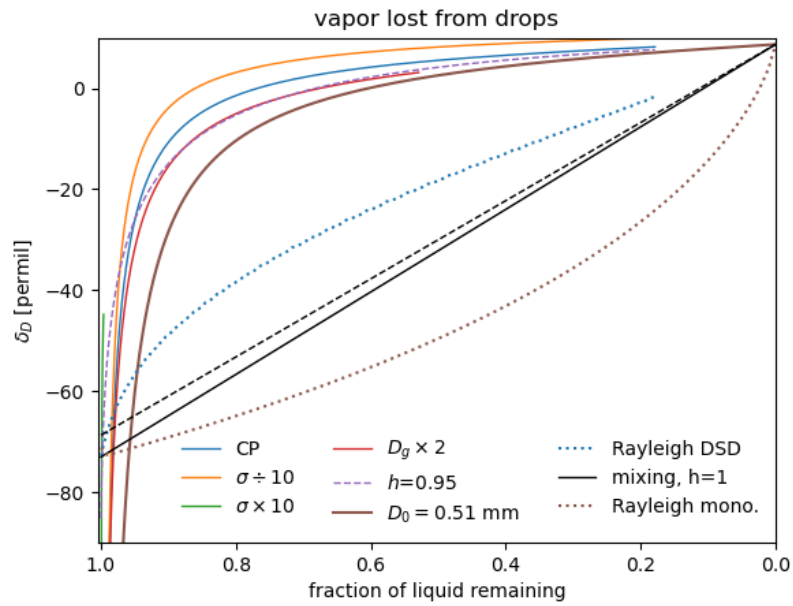
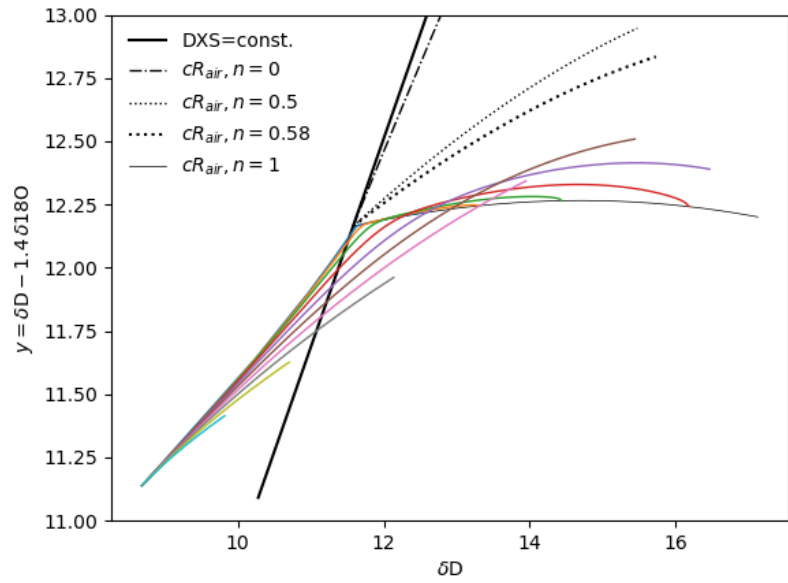












A Simple Model for the Evaporation of Hydrometers and Their Isotopes

Simon P. de Szoeko¹, Mampi Sarkar^{2,3}, Estefanía Quiñones Meléndez¹,
Peter N. Blossey⁴, David Noone^{1,5}

¹College of Earth, Ocean, and Atmospheric Sciences, Oregon State University, Corvallis, OR, USA

²Institute of Climate and Atmospheric Science, University of Houston, Houston, TX, USA

³Department of Earth and Atmospheric Sciences, University of Houston, Houston, TX, USA

⁴University of Washington, Seattle, WA, USA

⁵Department of Physics, University of Auckland, New Zealand

Key Points:

- Evaporated vapor from rain ($\delta_D = 0$ ‰ with 0.2 of rain mass evaporated) is near the rain's initial isotope composition, strongly enriched compared to the surrounding vapor.
- Rain isotope composition quickly equilibrates to the surrounding environmental vapor.
- Small and especially vanishing drops are enriched by molecular diffusion 40% more than millimeter-sized drops.

Abstract

Evaporation decreases the mass and increases the isotope composition of falling drops. Combining and integrating the dependence of the evaporation on the drop diameter and on the drop-environment humidity difference, the square of drop diameter is found to decrease with the square of vertical distance below cloud base. Drops smaller than 0.5 mm evaporate completely before falling 700 m in typical subtropical marine boundary layer conditions. The effect on the isotope ratio of equilibration with the environment, evaporation, and kinetic molecular diffusion is modeled by molecular and eddy diffusive fluxes after Craig and Gordon (1965), with a size-dependent parameterization of diffusion that enriches small drops more strongly, and approaches the rough aerodynamic limit for large drops. Rain shortly approaches a steady state with the subcloud vapor by exchange with a length scale of 40 m. Kinetic molecular diffusion enriches drops up to as they evaporate by up to +5 ‰ for deuterated water (HDO) and +3.5 ‰ for H₂¹⁸O.

Rain evaporation enriches undiluted subcloud vapor by +12 ‰ per mm rain, explaining enrichment of vapor in evaporatively cooled downdrafts that contribute to cold pools. Microphysics enriches the vapor lost by the early and complete evaporation of smaller drops in the distribution. Vapor from hydrometeors is more enriched than it would be by Rayleigh distillation or by mixtures of liquid rain and vapor in equilibrium with rain.

Plain Language Summary

A model of evaporating rain explains enrichment of rare isotopes in water vapor observed during atmospheric cold pools below shallow convection. Rain becomes more enriched as it evaporates by exchange with subcloud vapor, by equilibrium fractionation, and by the weaker molecular diffusivity of rare-isotope water vapor. The model predicts molecular diffusion enriches the rain drops more than previously thought, especially as they near complete evaporation.

1 Introduction

Clouds transport water from the subcloud boundary layer and condense and detrain it in and above the planetary boundary layer. Models for hydrometeor (cloud and rain drop) evaporation are useful for characterizing vapor sources and inferring cloud and rain processes. Condensation and evaporation processes fractionate the ratio of total water molecules to its rare isotopologues. (H₂¹⁸O contains the oxygen-18 [¹⁸O] isotope and deuterated water HDO contain the deuterium [D or ²H] isotope.) Combinations of sources and processes yield particular water vapor and precipitation isotope ratios (e.g., Dansgaard, 1964; Gat, 1996; Noone et al., 2012; Tremoy et al. 2014; Crawford et al. 2017), yet the problem of inferring the history of water from observed or modeled isotopes is confounded by complex and ambiguous combinations of sources and processes (Galewsky et al., 2016; Hiron and Flossman, 2020).

This complexity is reduced for idealized cases, such as mixing, Rayleigh distillation of water vapor by condensation, precipitation, and the predictable combination of vapor exchange, equilibrium fractionation, and diffusion accompanying evaporation (Craig and Gordon, 1965; Stewart, 1975). The equations predicting isotopic fractionation during rain evaporation in weather and climate models (Noone et al., 2012; Blossey et al., 2010; Risi et al., 2021; Sengupta et al., 2023) are numerically integrated to simulate observed cases and process studies (e.g., Salamalikis et al., 2016; Graf et al., 2017; Sarkar et al., 2023). The isotope ratio depends strongly on the fraction of the drop that evaporates, allowing the isotope evaluation to be conveniently separated from evolution of the drop mass (e.g., Hiron and Flossman, 2020).

65 Here we model the evaporation of hydrometeors (rain drops and cloud droplets)
 66 to interpret isotope observations in precipitation and water vapor observed in atmospheric
 67 cold pools (Quiñones Meléndez et al., 2024). The observations are summarized in sec-
 68 tion 2. A model for evaporation of atmospheric hydrometeors is presented that solves
 69 for isotope concentration of rain drops and of evaporated vapor from the drops, in sec-
 70 tion 3. Section 4 presents results of the model. The solutions show two regimes: In the
 71 *falling* regime a small fraction of the drop evaporates as it falls through the environment.
 72 In the *vanishing* regime the remaining hydrometeor completely evaporates as its fall speed
 73 goes to zero. A simulation is used to interpret rain and downdraft vapor observed dur-
 74 ing the EUREC4A-ATOMIC (Elucidating the role of clouds–circulation coupling in cli-
 75 mate - Atlantic Tradewind Ocean Mesoscale Interaction Campaign) field experiment (Stevens
 76 et al., 2021). Sensitivity experiments to initial conditions and microphysics demonstrate
 77 and isolate distinct effects on the isotopes by exchange with surroundings, equilibrium
 78 fractionation, and differential diffusion. Section 5 summarizes the article.

79 2 Observations of a cold pool

80 Compared to the varied processes that contribute to the isotope ratio of precip-
 81 itation and water vapor in the atmosphere, a relatively simple set of processes contributes
 82 to warm (nonfreezing) marine trade cumulus clouds, allowing us to isolate the effect of
 83 local water vapor sources. We simulate the hydrometeor evaporation leading to an at-
 84 mospheric cold pool observed under shallow winter tropical trade cumulus clouds over
 85 the western Atlantic Ocean during EUREC4A-ATOMIC (Quinn et al., 2021; Bailey et
 86 al., 2023; Quiñones Meléndez et al., 2024). Figure 1 shows the time series at 1-minute
 87 resolution of a cold pool observed on Feb 10, 2020 around 16:00 UTC aboard the NOAA
 88 research vessel *Ronald H. Brown*. With air temperature cooling by 2.5 °C, this cold pool
 89 is among the strongest events observed on the ship while isotope measurements were avail-
 90 able. Rain fell at the ship during the temperature front and minimum, suggesting the
 91 cold air and slight moistening of the specific humidity (Fig. 1b) were caused by the evap-
 92 oration of hydrometeors. Water vapor isotope ratios (δD and ^{18}O , Fig. 1c,d) are enriched
 93 in the cold pool compared to the background subcloud vapor measured before the cold
 94 pool. Three rain samples were promptly collected in rain showers at 16:15, 16:25, and
 95 16:40 UTC, and later analyzed to have $\delta_D = 15.5, 14.5, \text{ and } 16.2 \text{ ‰}$ and $\delta_{^{18}O} = 0.17,$
 96 $0.87, \text{ and } 0.4 \text{ ‰}$ (blue dots show the equivalent equilibrium vapor $\delta_{eq.v} = \alpha_e(\delta_L + 1) -$
 97 1 in Fig. 1c,d), with α_e computed at $T = 295 \text{ K}$. This is one of the strongest cold
 98 pools among those for which Quiñones Meléndez et al. (2024) analyzed the sources of
 99 potential temperature, specific humidity, and isotope ratio. Having synchronous and col-
 100 located observations of rain, cold temperature, and enriched isotope ratios, the Feb 10,
 101 16 UTC event excels for studying water vapor from freshly evaporated hydrometeors.

102 We construct a case for evaporation of hydrometeors below cloud, adopting initial
 103 conditions from Sarkar et al. (2023; called Sarkar23; Table 1). Drops are released from
 104 cloud base at 700 m and fall through a layer of uniform specific humidity with q_v 12.9
 105 g kg^{-1} . Because the temperature increases adiabatically downward, environmental rel-
 106 ative humidity is saturated at cloud base and 0.69 at the surface. The isotope ratio of
 107 the initial drop liquid $\delta_{D,L0} = 8.68 \text{ ‰}$ is taken to be in equilibrium with vapor ($\delta_{D,v0} =$
 108 -73 ‰) measured on the WP-3 aircraft (Sarkar et al., 2023).

109 We modify the subcloud layer water vapor in case CP slightly from Sarkar23 to match
 110 the background surface vapor of $\delta_{D,17m} = -69.7 \text{ ‰}$ observed before the cold pool (Fig. 1).
 111 Humidity and isotopes are taken to be mixed by subcloud layer-scale eddies above the
 112 surface layer. The height of the isotope analyzer inlet (18 m) is within the surface layer,
 113 so it will be more enriched than most of the subcloud layer due to gradients near the ocean
 114 (e.g., Thurnherr et al. 2020). We adjust humidity and isotopes by integrating the gra-
 115 dients through the constant-flux surface layer (Garratt, 1992), and average the result for

Figure 1. Ship time series containing a cold pool from 2020 Feb 10 15:40-17:00 UTC. (a) air temperature ($^{\circ}\text{C}$), rain rate (cyan shaded, mm h^{-1}), and (b) specific humidity (g kg^{-1}) at 17 m. (c) δ deuterium ($\text{‰} = 10^{-3}$) and (d) δ oxygen-18 sampled at 18 m. Rain liquid was collected promptly during rain showers at 16:15, 16:25, and 16:40; and subsequently analyzed. Vapor isotope ratio $\delta_v = \alpha_e(\delta_L + 1) - 1$ in equilibrium with the rain is shown by blue dots in (c) and (d).

Table 1. Initial conditions at cloud base (saturated) and subcloud vapor conditions for case Sarkar23 (Sarkar et al., 2023) and case CP (2020 Feb 10, 16 UTC). Subcloud air is adiabatically stratified and uniformly has the specific humidity and isotope ratio of the surface. Vapor in cloud and subcloud air are observed by aircraft for Sarkar23; the corresponding equilibrium liquid is computed. CP uses initial rain liquid from Sarkar23. CP observations of vapor from the isotope analyzer before the cold pool are adjusted to the subcloud mean with flux-gradient similarity theory; equilibrium liquid is computed. CP rain is observed and the corresponding equilibrium vapor is computed.

	z (m)	T (K)	q_v (g kg ⁻¹)	$\delta_{D,\text{liq}}$ (‰)	$\delta_{D,\text{vap}}$	$\delta_{18\text{O},\text{liq}}$	$\delta_{18\text{O},\text{vap}}$
case Sarkar23							
cloud base vapor	700	290	12.9	8.68	-73	-1.75	-11.7
subcloud vapor	0	296.8	12.9	4.54	-70	-1.14	-10.5
rain liquid modeled	0	296.8	-	15.8	-59.6	2.03	-7.36
case CP							
cloud base vapor	700	290	12.9	8.7	-73	-1.75	-11.7
subcloud vapor	0	296.8	12.9	4.1	-70.3	-1.02	-10.4
rain liquid modeled	0	296.8	-	15.4	-60.2	2.14	-7.24
rain liquid observed	0	296.8	-	15.4	-60.0	0.7	-8.7

116 150-700 m. This gives a subcloud deuterium isotope ratio of $\delta_{D,\text{subcloud}} = -70.3$ ‰,
 117 very close to Sarkar23's $\delta_{D,\text{subcloud}} = -70$ ‰ (Table 1).

118 3 Model

119 Following Best (1952; and, e.g., Abraham, 1962; Li and Srivastava, 2001), the prog-
 120 nostic drop evaporation model evaluates the change of the square of the drop diameter
 121 as a function of the temperature and humidity of the environment. The model param-
 122 eterizes diffusive kinetic effects that depend on empirical drop ventilation factors, the
 123 hydrometeor fall speed (Graf et al., 2017), and a vertically varying environment. We ob-
 124 tain analytical functions accurate within a neighborhood of drop diameter and height
 125 below cloud. Isotope ratios are calculated from the drop diameters with the Craig and
 126 Gordon (1965) model.

127 3.1 Drop diameter and mass

128 Sarkar et al. (2023) integrates prognostic equations for the mass, temperature, and
 129 isotope ratios of liquid water drops evaporating as they fall from cloud base to the sur-
 130 face for several drop size distributions and environmental profiles observed from the NOAA
 131 WP-3 aircraft in EUREC4A-ATOMIC (Pincus et al., 2022; Bailey et al., 2023). We sim-
 132 ulate the 2020 Feb 9 case, approximating the drop size distribution (DSD) by the log-
 133 normal distribution of Sarkar et al. (2023; section 3.4).

134 The Lagrangian prognostic equations for the drop are transformed from time deriva-
 135 tives to vertical derivatives by dividing by the fall speed $U_{\text{fall}} = -dz/dt > 0$. The equa-
 136 tion for drop diameter D evaporating into surrounding air with temperature T_a and va-
 137 por density $\hat{\rho}_{va}$ is (Salamalikis et al., 2016; Graf et al., 2017),

$$\frac{dD}{dz} = \frac{4f_v K_{va}}{DU_{\text{fall}} \hat{\rho}_l R_v} \left(\frac{e_s(T_r)}{T_r} - \text{RH} \frac{e_s(T_a)}{T_a} \right) = \frac{4f_v K_{va}}{DU_{\text{fall}} \hat{\rho}_l} (\Delta \hat{\rho}_v), \quad (1)$$

138 where f_v is the ventilation factor (Stewart, 1975), K_{va} the kinematic diffusivity of va-
 139 por in air, and T_r is the drop surface temperature and $e_s(T)$ is the saturation vapor pres-
 140 sure, RH is relative humidity, and $\Delta\hat{\rho}_v = \hat{\rho}_{vr} - \hat{\rho}_{va} > 0$ is the vapor density difference
 141 between the air and the drop surface. In this equation, $dD/dz > 0$ because the drops
 142 shrink as they fall.

143 We write equation (1) in terms of the uniform specific humidity, assuming a well-
 144 mixed subcloud layer and adiabatic temperature below cloud. The drop temperature ap-
 145 proaches the wet bulb temperature (Appendix B). Linearizing the saturation specific hu-
 146 midity and the wet-bulb temperature lapse rate Γ_w yields

$$\frac{dD}{dz} = \frac{4f_v K_{va}}{DU_{\text{fall}}\hat{\rho}_l} \left(\frac{\partial q_s}{\partial T} \right)_{\bar{T}} \Gamma_w z'.$$

147 Then, the drop evaporation equation is divided into one factor that depends on D on
 148 the left hand side, and another that depends on the vertical displacement from cloud base
 149 on the right hand side:

$$-a(D)D dD = z' dz', \quad (2)$$

150 with

$$a(D) = \frac{\hat{\rho}_l}{4K_{va}\Gamma_w(\partial q_s/\partial T)_{\bar{T}}} \frac{U_{\text{fall}}}{f_v}. \quad (3)$$

151 The factor a is nearly a constant, as the quotient U_{fall}/f_v is a slowly varying function
 152 of diameter. For drops larger than 0.5 mm $U_{\text{fall}}/f_v \approx 0.9 \text{ m s}^{-1}$. At smaller diameter,
 153 the fall velocity vanishes faster than the ventilation factor, and $a(D)$ (equation 3) be-
 154 comes very small.

155 Solutions of equation (2) describe elliptical arcs centered at $D = 0, z' = 0$ (Fig. 2).

$$-a(D^2 - D_0^2) = z'^2 - z_0'^2 \quad (4)$$

156 Best (1952) encapsulates the effect of the environment, mainly the saturation deficit, in
 157 a local “evaporation radius” K on the right hand side, $D_1^2 - D_2^2 = 4K^2$. The drop diameter-
 158 displacement curves are elliptical because saturation deficit increases linearly with dis-
 159 tance from cloud base $4K^2 = a^{-1}(z_2'^2 - z_1'^2)$. Small departures from the linear depen-
 160 dence on height such as fall speed and ventilation are contained in a . Numerical solu-
 161 tions of 4 show the curves of radius vs. height are nearly ellipses (Fig. 2b and Fig. 1 of
 162 Abraham et al., 1972), but flatten out as drops vanish and their fall speed goes to zero.

163 **Drop vanishing.** The function $a(D)$ varies little for $D > 0.4$ mm. But in the
 164 Stokes (1851) viscous drag regime, when drops get smaller ($\text{Re} < 5$), the fall speed $U_{\text{fall}} \propto$
 165 D^2 and $a(D)$ vanish over small vertical displacements. This squashing of the displace-
 166 ment near vanishing due to the dependence on U_{fall}/f_v , can be parameterized by the func-
 167 tion

$$a \approx a_0 \frac{D^2}{D^2 + b^2}, \quad (5)$$

168 with $a_0 = 2.1 \times 10^{12}$ and $b = 0.2$ mm. This approximation estimates the displace-
 169 ment at which drops vanish. The vanishing factor $D_1^2/(D_1^2 + b^2)$ approaches unity in
 170 the falling regime.

171 The quasi-elliptical trajectories of drop diameter vs. displacement fallen can be eval-
 172 uated in midpoint prediction-correction steps of drop diameter. It is accurate to evalu-
 173 ate in a few ($k_{\text{max}} = 5$) cosine-spaced steps $D_k = D_0 \cos(\pi k/(2k_{\text{max}}))$ (Fig. 2b, cir-
 174 cles). However, to find the resulting size of all drops at each height, we use 1 m verti-
 175 cal resolution (Fig. 2b, lines). The 5-step evaluation agrees with the high-resolution so-
 176 lution because the slope $a(D)$ varies slowly. A single step ($k_{\text{max}} = 1$) overestimates the
 177 displacement that small drops fall because of the curvature of $a(D)$ for $D \lesssim b \approx 0.2$ mm.
 178 The approximation for a (equation 5) accurately predicts the displacements at which drops
 179 completely evaporate.

Figure 2. (a) The lognormal drop number $N(D)$ and mass size distributions. (b) Traces of individual diameters D from initial cloud-base ($z = 700$ m) diameters D_0 by numerical stepping of the quadratic equation. (c) Mass fraction remaining as a function of height and initial diameter. The dashed line shows $D = 0.14$ mm where $Re \approx 5$, for which drops with smaller diameters rapidly vanish in small displacements.

3.2 Isotope exchange

The change in the isotope ratio of a single liquid drop is calculated from the mass fraction $f = (D/D_0)^3$ of drop liquid remaining, using the Craig and Gordon (1965; and Stewart, 1975) model. Single-drop results are then integrated over the drop size distribution.

Craig and Gordon (1965) and Stewart (1975) assume finite diffusion between the equilibrium vapor over the drop and the surrounding air. The drop isotope ratio R_L is predicted by

$$R_L - cR_{air} = (R_{L0} - cR_{air})f^A, \quad (6)$$

where f is the mass fraction of the drop remaining. The exponent is

$$A = \frac{\rho}{\rho_i} \frac{\alpha_e}{1-h} - 1.$$

where $\alpha_e = R_V/R_L < 1$ is the (equilibrium) fractionation factor of vapor over liquid. The coefficient c is

$$c = \frac{h}{\alpha_e - (1-h)(\rho_i/\rho)}. \quad (7)$$

Including exchange with environmental vapor and diffusive effects replaces α_e in the Rayleigh process with $\alpha_e(\rho/\rho_i)/(1-h)$. Rayleigh evaporation assumes vapor at equilibrium over the drop irreversibly leaves the drop as it evaporates. The isotope ratio of the liquid is then fractionated (Rayleigh):

$$R_L = R_{L0}f^{\alpha_e-1}.$$

The initial condition for equation 6 is $f = 1$. As $f \rightarrow 0$,

$$R_{Lend} = cR_{air}. \quad (8)$$

For saturation fraction $h = 0$, cR_{air} drops out, giving $R_L = R_{L0}f^{\alpha_e\rho/\rho_i-1}$, which is like the Rayleigh solution, except for ρ/ρ_i in the exponent.

3.3 Kinetic effect of diffusion from evaporating drops

A spherical drop evaporates by a sum of diffusion by molecular diffusivity K_m and eddy diffusivity K_e . The molecular diffusivity varies for different isotopes, the eddy diffusivity K_e depends on the flow around the drop, but is the same for all species. Moreover, the ratio of resistances $\rho_i/\rho = 1 + n(K_m/K_{mi} - 1)$ of flux of the rare isotope to the flux of abundant water vapor depends on the drop size through the ratio of molecular to total (molecular + eddy) resistance $n = \rho_m/\rho$. The diffusivity ratio K_{mi}/K_m from Merlivat (1978) is 0.9755 for deuterium and 0.9723 for oxygen-18. Stewart (1975) and Kinzer and Gunn (1951) found $n = 0.58$ for drops in the range 1.4-2.8 mm diameter.

For spherical symmetry and steady conditions, the drop evaporation flux E is a product of the diffusivity K and the radial derivative of saturation fraction $h = \hat{\rho}_v/\hat{\rho}_{vsat}$,

$$E = -\frac{1}{\hat{\rho}_{vsat}} \frac{dm}{dt} = -4\pi r^2 K \frac{dh}{dr},$$

where $\hat{\rho}_v$ is vapor density. Integrating the humidity h from the drop surface radius a where $h = 1$ gives the humidity $h(r)$ as a function of distance from the drop,

$$1 - h(r) = \int_r^a dh = \frac{E}{4\pi} \int_r^a \frac{1}{K} \frac{dr'}{r'^2} = \frac{E}{4\pi} \frac{1}{K} \left(\frac{1}{a} - \frac{1}{r} \right). \quad (9)$$

212 We model the diffusion through spherical shells, with molecular diffusivity K_m from the
 213 drop radius a through a laminar layer of thickness l , and with eddy diffusivity K_e out-
 214 side radius $a + l$. The area-integrated nondimensional vapor flux through the shell is,
 215 uniform with radius, $E = (1 - h)/\rho$. It depends only on the saturation deficit and re-
 216 sistance $\rho = 1/(4\pi K a)$.

217 Integrating at shells of different radii gives $\rho = \rho_m + \rho_e$ with

$$\rho_m = \frac{1}{4\pi K_m a} \frac{l}{a+l} \text{ for } r = [a, a+l],$$

218 and

$$\rho_e = \frac{1}{4\pi K_e} \frac{1}{a+l} \text{ for } r = [a+l, \infty).$$

219 This spherical model of diffusion yields the ratio of molecular to total resistance,

$$n = \frac{\rho_m}{\rho} = \left(1 + \frac{K_m a}{K_e l}\right)^{-1},$$

220 that depends on the ratio a/l of the drop size to a viscous-diffusive length scale l . Va-
 221 por diffuses away from small drops through concentric shells, as above, in a laminar layer
 222 of thickness $l_\nu = \nu/U$. The velocity U balances drag with gravity and turbulent iner-
 223 tial accelerations.

224 Diffusion through this spherical geometry predicts vanishingly small drops approach
 225 $n = 1$. Flow separates from large drops and the diffusion loses its spherical geometry.
 226 Choosing total thickness

$$l = l_\nu + l_e,$$

227 with $l_e = (K_m/K_e)a$, matches the rough limit $n = 1/2$ for large drops (Brutsaert, 1965;
 228 1975; Merlivat and Jouzel, 1979). Molecular to eddy vapor diffusivity ratio $K_m/K_e =$
 229 6×10^{-3} matches the experimental results, for drops of diameter 1.4, 2.1, and 3 mm,
 230 of Kinzer and Gunn (1951) and Stewart (1975) (Fig. 3 solid). We use this first param-
 231 eterization. An ad hoc alternative parameterization matching the experiments, that asymp-
 232 totes instead to $n = 0.55$ for large drops, is $\tilde{n} = 0.55 + 0.45(1 + 0.04a/l_\nu)^{-1}$ (Fig. 3
 233 dashed).

234 Models such as Lee and Fung (2008), Graf et al. (2019), and Sarkar et al. (2023)
 235 include the effect of differential diffusion through empirical ventilation factors that de-
 236 pend on the diffusivity of each isotopologue species. Our approach follows Stewart (1975),
 237 resolving kinetic effects by explicitly parameterizing the flow- and geometry-dependence
 238 of the ratio of laminar and turbulent resistances. Where Stewart had determined this
 239 experimentally for 1-3 mm drops, we parameterize the effect as a function of the size of
 240 any falling drop. This explicit treatment of diffusivity predicts kinetic effects on the iso-
 241 topes of drops even as they vanish.

242 3.4 Drop size distribution

243 We evaluate the diameter of drops sampled from a drop size distribution (DSD).
 244 The initial DSD is the lognormal distribution

$$N(D_0) = N_0/(D_0\sqrt{2\pi\sigma^2}) \exp(-(\log(D_0) - \mu)^2/(2\sigma^2)), \quad (10)$$

245 observed from aircraft in Atlantic trade wind shallow cumulus clouds in EUREC4A-ATOMIC.
 246 The drop number concentration $N_0 = 500 \text{ m}^{-3}$, the lognormal width is $\sigma = 0.35$, and
 247 the lognormal mode $\mu = \log(D_g)$ is the log of the geometric mean diameter $D_g = 0.22$
 248 mm, equivalent to the DSD of Sarkar et al. (2023), but with alternate notation. Figure 2a
 249 shows this DSD. Substitution of D from equation 4 could be used to derive the evolu-
 250 tion $N(D)$ of the DSD with time. However, since resolving the vanishing behavior of drops

Figure 3. Resistance ratio $n = \rho_m/\rho$ parameterization (solid), ad hoc empirical parameterization n_{emp} (dashed), with lab experiment results of Kinzer and Gunn (1951; circles) and Stewart (1975; circle and whisker).

Figure 4. (a) Mass fraction of total liquid remaining vs. height. (b) Mean deuterium δ (‰) of all the liquid remaining. (c) Deuterium δ of drop evaporation at each height (dot-dashed) and cumulative evaporated vapor (solid). Black dashed (c) shows the isotope ratio of the surrounding vapor.

251 is important, we explicitly simulate predict the diameter change of 161 drops, initially
 252 geometrically spaced with diameters D_0 between 11×10^{-6} m and 33 μ m. This set of
 253 drops resolves the tails of the DSD. Drop diameters D are evaporated by equation 4. Drops
 254 initially smaller than $D_{0\text{crit}} = 0.51$ mm evaporate completely within 700 m below cloud
 255 base.

256 4 Isotope results

257 We evaluate the isotope ratio R_L of each drop using the mass fraction f and equa-
 258 tion 6 for the cold pool case (CP, Table 1). The total mass fraction, and deuterium com-
 259 position of the remaining DSD and the vapor lost is shown in Fig. 4. Figure 4c shows
 260 the deuterium composition of the immediately evaporated vapor (dot-dashed) and the
 261 cumulative vapor (solid), compared to the surrounding subcloud vapor (black dashed)
 262 in delta notation $\delta = R/R_{\text{standard}} - 1$. The cumulative vapor below 650 m is enriched
 263 compared to the surroundings. It is enriched to $\delta = 0$ ‰ below 500 m. A small frac-
 264 tion of this enriched vapor could explain the enrichment observed in cold pools in Fig. 1.
 265 The immediately evaporated vapor at each level is yet more enriched.

266 The isotope ratio is shown for 10 drops with diameters of 0.13 to 4.8 mm (Fig. 5).
 267 The initial isotope ratio is $\delta_{\text{DL0}} = 8.68$ ‰, $\delta_{\text{isOL0}} = -1.75$ ‰ (‰ $\equiv 10^{-3}$). Drops en-
 268 rich monotonically as they fall and evaporate fractionally more of the lighter H_2O iso-
 269 topologues. Curves that strike $z = 0$ reach the surface. The largest drop shown (4.8
 270 mm; cyan left) nearly reaches $\delta_{\text{D}} = 10$ ‰ at the surface. Smaller drops fall slower, evap-
 271 orate fractionally more and become more enriched over a shorter distance. The small-
 272 est drop shown (blue, top) quickly reaches equilibrium with the surrounding vapor, be-
 273 fore evaporating completely between 500-600 m. The largest drop shown here that evap-
 274 orates completely (0.44 mm, red) enriches to $\delta_{\text{D}} = 16$ ‰, where it vanishes around 150
 275 m. The enrichment curves for water containing deuterium or oxygen-18 isotopes appear
 276 quite similar, differing mostly due to the difference between isotope ratio of the initial
 277 drop and the equilibrium liquid isotope ratio of the air (at the intersection of the black
 278 lines at cloud base), which is stronger, relative to its kinetic effect, for deuterium than
 279 for oxygen-18.

280 All drops enrich by exchange with the surrounding vapor, from the drop initial con-
 281 dition, toward equilibrium with the vapor. The equilibrium liquid isotope ratio of the
 282 air at $h = 1$ (shown at $z=700$ m) is $\delta_{\text{D, end}} = 11.6$ ‰, $\delta_{\text{isO, end}} = -0.42$ ‰ for subcloud
 283 air vapor isotope ratios $\delta_{\text{D, air}} = -70.3$ ‰, $\delta_{\text{isO, air}} = -10.4$ ‰. Large drops fall through
 284 the layer exchanging only slightly, while small drops exchange quickly toward equilib-
 285 rium with the enriched ambient vapor. Lee and Fung (2008) use the rate at which drops
 286 reach isotopic equilibrium with relatively enriched environmental vapor as a possible ex-
 287 planation for the amount effect phenomenon, where precipitation is relatively depleted
 288 at higher precipitation rates (Dansgaard, 1964).

289 In addition to exchange and equilibration, kinetic effects (Fig. 5) result in small
 290 drops reaching a yet more enriched end point at lower relative humidity, where the “end
 291 point” is the asymptotic value of the raindrop isotopic composition as $D \rightarrow 0$. The heav-
 292 ier water isotopologues diffuse away from the drops more slowly than H_2^{16}O , enriching

293 them. The black lines show the end point isotope ratio of liquid drops predicted by differ-
 294 ent parameterizations of the kinetic fractionation (i.e. different values of n). At cloud
 295 base (700 m, $h = 1$) all endpoint curves intersect the vertex of equilibrium with the en-
 296 vironmental vapor. Drops approach their end point isotope ratio $R_{\text{end}} = cR_{\text{air}}$ (thin
 297 black line) predicted by equation 7. The kinetic effect of differential diffusion is stronger
 298 as n approaches unity, for small drops. The isotope ratio $R_{\text{air}}h/[\alpha_e - (1 - h)]$ (black
 299 dot-dashed) is the end point for the artificial case of $n = 0$, which would be obtained
 300 were the isotope diffusivity equal the ordinary vapor diffusivity.

301 Estimates of R_{end} , using our n parameterization to model ρ_i/ρ , for large (4.8 mm)
 302 drops (black solid), agree with results for $n = 0.58$ (black dashed), found for lab ex-
 303 periments on drops larger than 1 mm diameter (Stewart, 1975). The $n = 0.58$ end point
 304 underestimates kinetic enrichment as drops shrink. Even drops as small as 0.13 mm fall
 305 more than 100 m with their isotope ratio greater than the endpoint R_{end} predicted by
 306 $n = 0.58$. The enrichment of δ_{end} is approximately proportional to n . Our parameter-
 307 ization for n , which approaches $n = 1$ and ($\rho_i/\rho = K_m/K_{mi}$) for small drops has about
 308 42% more kinetic enrichment than taking constant $n = 0.58$.

309 Though the mass of vanishing drops is small, rain transports enriched liquid down-
 310 ward, leaving relatively depleted vapor near cloud base. Small drops and virga experi-
 311 ence the strongest enrichment and their complete evaporation moves very enriched vapor
 312 downward in the subcloud layer. Virga that evaporates just before reaching the sur-
 313 face is enriched, by +7 ‰ for deuterium and by +5 ‰ for oxygen-18, with kinetic effects
 314 of +5.8 ‰ and +3.5 ‰, respectively. This evaporation of enriched hydrometeors (both
 315 large and small) explains enrichment of vapor observed in evaporatively cooled cold pools
 316 in EUREC4A-ATOMIC (section 2).

317 Equilibration and kinetic effects reduce deuterium excess (DXS, Fig. 6) of drops
 318 as they fall, because the loss to evaporation of HDO is more efficient than the loss of H_2^{18}O ,
 319 enriching the drops relatively more in H_2^{18}O than predicted by the global meteoric wa-
 320 ter line. DXS of the equilibrium ($n = 0$) end point is 8 ‰ lower in the subcloud vapor
 321 than in the initial drop condition, but the DXS is reduced by 20 ‰ by drops that un-
 322 dergo significant kinetic enrichment.

323 The rain evaporation process, replete with kinetic evaporation, does not describe
 324 a meteoric water line with nearly constant DXS = $\delta_{\text{D}} - 8\delta_{18\text{O}}$. Figure 7 shows isotope
 325 δ trajectories of evaporating drops have continuously decreasing DXS. The first adjust-
 326 ment from initial liquid ($\delta_{\text{D}} = 8.7$ ‰) toward 11.6 ‰ is due to exchange with the sur-
 327 rounding vapor, so its slope depends strongly on those prescribed conditions, rather than
 328 on any physical process. In the kinetic enrichment limit for small drops ($n \rightarrow 1$), δ_{D}
 329 increases in proportion to $1.4\delta_{18\text{O}}$. As drops vanish, they approach a nearly constant $y =$
 330 $\delta_{\text{D}} - 1.4\delta_{18\text{O}}$ of the surrounding vapor, of about $y_{\text{end}} = 12.1$ ‰. The limits $\delta_{\text{end}} = cR_{\text{air}}/R_{\text{std}} -$
 331 1 for deuterium and oxygen-18 of small drops and constant subcloud vapor R_{air} shows
 332 the linearity of δ_{D} and $\delta_{18\text{O}}$ (Figure 5) depends on the ratio of $c_{\text{D}}/c_{18\text{O}}$. Changes in sat-
 333 uration h over the drop and $\alpha_e(T)$ with height are responsible for the compensated changes
 334 of δ_{D} and $1.4\delta_{18\text{O}}$ along y_{end} .

335 4.1 Vapor lost by hydrometeors

336 The instantaneous and cumulative isotope ratio of the vapor evaporated from all
 337 hydrometeors in the DSD is shown as a function of height in Fig. 4b and c, and as a func-
 338 tion of the mass fraction of original hydrometeor liquid in 8. Experiments show the iso-
 339 tope ratio of the vapor lost by the drops is dominated by equilibrium and kinetic frac-
 340 tionation, and secondarily by the DSD. The Craig and Gordon evaporation equation (CG;
 341 equation 6) generates concave-down curves that enrich quickly at first, i.e., at low mass
 342 fraction evaporated, and then slowly approach the isotope ratio of the original liquid δ_{D0} .
 343 The CG model for a single drop, or equivalently a monodisperse DSD (brown), is still

Figure 5. (a) Deuterium and (b) oxygen-18 isotope trajectories (colored lines) for drop with initial diameter D_0 of 0.13 (blue, top), 0.20, 0.29, 0.44, 0.65, 0.97, 1.45, 2.2, 3.2, and 4.8 (cyan, lowest) mm. Our parameterization for the end point $R_{\text{end}} = cR_{\text{air}}$ for vanishing drops with $n \rightarrow 1$ (thin black). No kinetic effect $\rho_i/\rho = 1$, $n = 0$, equilibrium fractionation only (dot-dashed black). R_{end} for $n = 0.5$ (thin dotted black) and $n = 0.58$ (Stewart, 1975; dotted black), which matches extrapolating our model for diffusion of large (4.8 mm) drops (black solid).

Figure 6. Deuterium excess $\text{DXS} = \delta_D - 8\delta_{18O}$ profiles as in Fig. 5.

Figure 7. Isotopic trajectory of the kinetic evaporation process. The vertical axis is $y = \delta_D - 1.4 \delta_{18O}$. Black lines represent constant DXS (thick solid), and the steady state endpoints as in Figs. 5-6. Vanishing drops tend toward a nearly constant y .

344 concave-down. The shape of these curves is mostly due to the CG physics, not the shape
345 of the DSD.

346 **4.1.1 Sensitivity to the DSD**

347 The standard ($D_g=0.22$, $\sigma=0.345$) drop size distribution is shown in blue. Results
348 are not sensitive to narrowing the DSD's lognormal width σ by a decade, or doubling
349 the geometric diameter D_g . The orange curve shows a narrower distribution, with width
350 $\sigma=0.0345$ decimated. A wider $\sigma=3.45$ distribution barely evaporates, and almost all liq-
351 uid remains at the surface (green; almost invisible at left), because much of the mass is
352 in drops too large to evaporate. The effect of the width on the isotopes is not monotonic:
353 The narrower and wider distributions both evaporate less and enrich faster than the stan-
354 dard DSD.

355 Doubling D_g to 0.44 mm (red) reduces fraction of rain evaporated between cloud
356 base and the surface to $f \simeq 0.55$. Vapor also enriches slightly more slowly, suggesting
357 relatively more evaporation from larger less enriched drops than from the control DSD.

358 A case with a single drop, equivalent to a monodisperse DSD, shows the vapor re-
359 sulting from the initial drop size ($D_0=0.51$ mm) that completely evaporates at the sur-
360 face. Preferential and near-complete evaporation of the smaller drops of the DSD are re-
361 sponsible for about +10 ‰ more enrichment of the cases with a DSD, compared to the
362 case with a single drop.

363 **4.1.2 Sensitivity to the environmental profile**

364 The case indicated by the dashed purple line uses uniform $h = 0.95$ (representa-
365 tive of 400 m), to simplify the effect of the environment. The main difference is that it
366 starts off evaporating near isotopic equilibrium, compared to the transient strongly de-
367 pleted vapor right below cloud base where h is nearly unity (blue line, off scale). Away
368 from cloud base, the uniform environment has only a small effect on the isotope ratio
369 of the evaporated vapor.

370 **4.1.3 Comparison to simpler models**

371 The simplest model for the isotope ratio of vapor is linear mixing between the ini-
372 tial liquid and its equilibrium vapor. Mixtures between the “first whiff” of initial equi-
373 librium vapor, and the “final gulp” of completely evaporated drops appear between the
374 straight black lines. The equilibrium varies slightly with h : the lower (solid) mixing line
375 represents equilibrium at cloud base $h = 1$, and the upper dashed line represents the
376 equilibrium at the surface $h = 0.89$.

377 The Rayleigh model for a single drop is concave up (purple dotted). This single-
378 drop Rayleigh model performs worse than linear mixing (black lines). Rayleigh evapo-
379 ration for drops in the EUREC4A-ATOMIC DSD (blue dotted) is concave down. Ac-
380 counting for the DSD, the Rayleigh model is significantly improved, falling between be-
381 tween linear mixing and the more physical CG solutions. The vapor equilibration and
382 kinetic fractionation effects additionally included in the CG model have a stronger ef-
383 fect on the results than the DSD. Evaluating CG even for a single average-sized drop gives
384 a considerably better result than the Rayleigh model.

385 **4.2 The rain isotope flux and source**

386 Figures 4 and 8 show the integrated effect of rain is to enrich rainwater quickly be-
387 low cloud (because the initial rain isotopic composition was in equilibrium with some-
388 what more depleted cloud layer air), and then evaporate this enriched water lower in the

Figure 8. Total isotope δ of vapor evaporated from rain drops, as a function of fraction f of rain mass remaining, modeling microphysical evaporation of drop mass, Craig and Gordon isotope evaporation model, with diameter-dependent kinetic effect (blue). Sensitivity studies have DSD with $10\times$ narrower (orange) or wider (green) lognormal width σ , $2\times$ larger geometric mean diameter D_g , surroundings with fixed T and $h = 0.95$ representative of 400 m (purple dashed), and for the single drop of initial diameter of 0.51 mm (brown). Mixtures of $f = f_{\text{eq}}$ equilibrium vapor from negligibly evaporated drops and $1 - f = f_{\text{complete}}$ vapor from completely evaporated drops of initial liquid isotope ratio (black: solid for vapor equilibrium over the drop evaluated at cloud base [700 m] and dashed for vapor equilibrium evaluated at the surface). Rayleigh evaporation of the control case DSD (blue dashed), and a monodisperse DSD (single drop, brown dashed).

389 subcloud layer. This suggests a downward flux of heavy isotopes by the rain. This up-
 390 gradient flux acts to strengthen the observed depletion of heavy isotopes with altitude
 391 in the atmosphere.

392 The vertical flux of water isotopes by the rain is quantified from the model sim-
 393 ulations:

$$F_{\delta\text{rain}} = \sum_j M_j(\delta_j - \bar{\delta}), \quad (11)$$

394 where $M_j = -(\pi/6)\hat{\rho}_l D_j^3 U_{\text{fall},j} N_j$ is the mass flux of drops of diameter D_j with the drop
 395 number concentration of per unit volume of air, $N_j = N(D_{0,j})$, given by the initial DSD.

396 In our steady state model, the total water isotope source, to the air-rain mixture
 397 due to the rain, is the convergence of the rain isotope flux,

$$S_{\delta\text{rain}} = -\frac{1}{\hat{\rho}_v} \frac{\partial}{\partial z} F_{\delta\text{rain}} = \frac{1}{\hat{\rho}_v} \sum_j \left[-\frac{\partial M_j}{\partial z} (\delta_j - \bar{\delta}) - M_j \frac{\partial}{\partial z} (\delta_j - \bar{\delta}) \right], \quad (12)$$

398 where $\hat{\rho}_v$ is the vapor density per unit of total air and $\bar{\delta}$ is the mean isotope δ of total
 399 water, which is dominated by the subcloud vapor. The source is separated into two phys-
 400 ically distinct parts: on the left, the effect of bulk rain evaporation, and on the right, the
 401 effect of advection of the isotopes by the rain.

402 The mass flux, isotope flux, and source rates all scale with the rain rate (and N_0);
 403 the integrated source scales with the rain accumulation. We evaluate the rain flux of δ
 404 for the deuterium isotope for a nominal rain rate of $M_j/\hat{\rho}_l = 1 \text{ mm h}^{-1}$ (Fig. 9a), and
 405 the integrated source for 1 mm of precipitation accumulation at the surface (Fig. 9b)

406 The weaker term of the flux divergence is the advection of the isotope by the rain.
 407 Since the mean $\bar{\delta}$ is nearly constant, the effect of the advection term is mostly within the
 408 liquid phase. Drops enrich by evaporation and exchange, especially near cloud base, caus-
 409 ing strongly negative $\partial\delta_j/\partial z$. This gradient results in negative isotope advection by the
 410 falling rain.

411 The stronger term is the evaporation (Fig. 9b, red). Removing rain mass causes
 412 convergence of the rain mass flux. Drops are enriched compared to the subcloud vapor,
 413 explaining the large enrichment by the evaporation. The vertically averaged subcloud
 414 rain evaporation source enriches an undiluted precipitating core by +11.8 ‰ per mm rain.
 415 The precipitation accumulation for the cold pool on Feb 10, 16 UTC (Fig. 1a) is 1.9 mm.
 416 Evaporation from this accumulation would enrich precipitation downdraft core by air
 417 by 22 ‰. This contributes to the cold pool, whose deuterium δ is enriched by +4.9 ‰ (Fig. 1c).
 418 Were the hydrometeor evaporation the only source, dilution of the evaporative core by
 419 3.6 times as much surrounding air would explain the vapor isotopes observed in the cold
 420 pool. In fact, other sources in addition to hydrometeor evaporation, such as evaporation
 421 from the ocean surface, also contribute to the near surface air in cold pools (Quiñones
 422 Meléndez et al. 2024).

423 4.3 Sensitivity to isotope ratio of the initial drop and subcloud vapor

424 The rain at the surface is largely equilibrated through exchange with the vapor in
 425 the subcloud air. This exchange was identified in early isotope-enabled general circula-
 426 tion models as a factor for predicting local precipitation-temperature relationships (e.g.,
 427 Noone and Simmonds, 2002). Experiments varying the initial drop isotope ratio, and vary-
 428 ing the isotope ratio of the vapor in the subcloud air show the isotope ratio of the sur-
 429 face rain (integrated over the DSD) depends strongly on the isotope ratio of the vapor
 430 in the air, and slightly on the drop initial conditions. The sensitivity for deuterium anoma-
 431 lies is

$$\delta'_{\text{pcp,sfc}} = 0.972\alpha_e^{-1}\delta'_{\text{air}} + 0.036\delta'_{L0}, \quad (13)$$

with $\delta' = \delta - \delta^\circ$ indicating anomalies from reference conditions δ° , which are for the standard cold pool case: $\delta_{\text{pcp,sfc}}^\circ = 15.4 \text{ ‰}$, $\delta_{\text{air}}^\circ = -70.3 \text{ ‰}$, and $\delta_{L0}^\circ = 8.68 \text{ ‰}$. The coefficients are constant over a wide range of observed conditions: $\delta_{\text{air}} = [-69, -72] \text{ ‰}$ and $\delta_{L0} = [9, 12] \text{ ‰}$.

4.4 Idealized experiments

Sensitivity experiments illustrate the effects of exchange with the environmental vapor, equilibrium fractionation, and kinetic diffusion on the isotopes. The same drop sizes as in Case CP are reused for all the experiments. In the first three experiments, the initial drop liquid and environmental vapor in the air are in isotopic equilibrium. The Control case has all three effects on the isotopes: exchange with the environmental vapor, equilibrium fractionation, and kinetic diffusion. The second case (OnlyDiff) has only environmental exchange and differential kinetic diffusion. Its equilibrium fractionation $\alpha_e = 1$ is artificially set to unity to suppress equilibrium fractionation. The third case (OnlyEq) has only environmental exchange and equilibrium fractionation. Its molecular diffusivity ratio K_m/K_{mi} is set to unity to suppress the diffusive kinetic effect. All the experiments have environmental exchange. Since these three cases have uniform subcloud air with $\delta = 0$, in equilibrium with the liquid drops ($\alpha_e^{-1}R_{\text{air}} = R_L = R_s$), environmental vapor exchange has the effect of simply relaxing back to $\delta = 0$.

Trajectories for drops with initial diameter $D_0 = 0.51 \text{ mm}$, which evaporate completely just above the surface, are shown for these four experiments in Fig. 10. The black lines are the steady state end points for $n = 0, 0.5$, and 1, as in Fig. 5. The steady state end point depends on relative humidity over the drop h , which goes from 1 at cloud base to 0.89 at the surface.

The Control experiment (blue, Fig. 10), with all 3 effects, reaches the end point of $\delta_D > 5 \text{ ‰}$ defined by $n = 1$. Differential isotope diffusion (OnlyDiff) and equilibrium fractionation (OnlyEq) mechanisms both enrich drops by similar amounts and the linear sum of these effects is only slightly less than their combined effect in the Control experiment. For kinetic diffusion without equilibrium fractionation (OnlyDiff: orange, Fig. 10), δ approaches a final value of $+3 \text{ ‰}$. For equilibrium fractionation without diffusion (OnlyEq: green, Fig. 10), $\rho_i/\rho = 1$ is achieved by $K_m/K_{mi} = 1$, and isotopes increase by $+2 \text{ ‰}$, reaching the end point for $n = 0$ (black dot-dashed). Setting $n = 0$ also excludes differential diffusion. The end points increase downward due to decreasing relative humidity. About half of the effect of relative humidity on the end point is counteracted by reduction of $\alpha_e^{-1} = \alpha_{eL/V}$ with increasing temperature.

These experiments (Control, OnlyDiff, OnlyEq; Fig. 11) are repeated for the environmental air depleted by $\delta = -1 \text{ ‰}$ relative to equilibrium over the initial drop. The exchange process immediately acts to deplete the drops toward $\delta = -1$. A fourth case (NoEqNoDiff, red Fig. 11) with only environmental exchange (having both equilibrium fractionation and differential diffusion disabled by setting to unity $\alpha_e = 1$ and $K_{mi}/K_m = 1$) illustrates this, relaxing to $\delta_{v,\text{air}} = -1 \text{ ‰}$ with a length scale of 40 m below cloud base, even for the relatively large drop ($D_0 = 0.51 \text{ mm}$). If $\delta_{l0} = \delta_{v,\text{air}} = 0$ then the drop in NoEqNoDiff would trivially maintain $\delta = 0$ (not shown).

Experiments Control, OnlyDiff, and OnlyEq for this relatively depleted environment also are initially depleted by the exchange. After the initial depletion, the drops in the experiments enrich by equilibrium fractionation and/or differential diffusion processes, respectively, for each experiment. The depleted environmental vapor also shifts the end points by -1 ‰ . As before, OnlyEq approaches the end point for $n = 0$, and Control approaches the end point for $n = 1$.

The depletion by exchange process opposite the enrichment by the equilibrium and diffusion processes results in non-monotonic adjustment that depends on the drop size

Figure 10. Deuterium isotope δ of drops of initial diameter $D_0 = 0.51$ mm and isotope ratio $\delta = 0$ for three experiments with air in isotopic equilibrium with the initial drop liquid isotope ratio $\delta_{L0} = \delta_{air} = 0$ ‰: Control (solid blue) includes exchange, equilibrium fractionation, and differential diffusion; OnlyDiff (orange) includes equilibrium and diffusion; and OnlyEq (green) includes exchange and diffusion. The dashed blue line shows the linear superposition δ sum of OnlyDiff and OnlyEq.

Figure 11. Deuterium isotope experiments Control (solid blue), OnlyDiff (orange), and OnlyEq (green) as in Fig. 10 but with environmental air depleted by -1 ‰ compared to equilibrium over the drop. A fourth experiment, NoEqNoDiff (red), has only exchange with air. Purple lines show results for different drop sizes, with smaller drops adjusting over shorter displacements.

482 (purple, Fig. 11). Smaller drops exchange faster, reach a minimum isotope ratio, then
 483 enrich faster by isotopic equilibrium fractionation and diffusion. Larger drops fall fast
 484 and adjust relatively slowly. Thus the isotope ratio trajectories cross for drops of differ-
 485 ent initial sizes.

486 The sensitivity studies demonstrate that the exchange and kinetic effects in the CG
 487 evaporation model make a significant difference to the results. The CG model is not sig-
 488 nificantly more complex than a Rayleigh model. Microphysics also makes a difference:
 489 Changing the DSD determines which drops evaporate completely having a profound ef-
 490 fect on the resulting vapor.

491 5 Conclusion

492 When rain evaporates below cloud base, the *liquid* nearly reaches an equilibrium
 493 by exchange with vapor in the surrounding air. This equilibrium is not the thermody-
 494 namic “saturation” equilibrium of vapor enclosed over a liquid surface, but rather is anal-
 495 ogous to the wet bulb temperature that drops also approach. The nearness of the drops
 496 to this equilibrium with their surroundings results in surface precipitation whose isotope
 497 ratio is mainly determined by the subcloud vapor. This exchange of the rain with rel-

498 atively enriched subcloud vapor explains the observed correlation of the precipitation iso-
 499 tope ratio to the local surface humidity (Crawford et al. 2017).

500 On the other hand, the hydrometeor source of *vapor* to the air is nearly the origi-
 501 nal liquid, because the bulk of the water mass evaporated is from large fractions of evap-
 502 oration of individual drops. The temporary enrichment of vanishing drops, and its en-
 503 hancement by diffusion, is an interesting flourish in the process that does not ultimately
 504 change the isotope ratio of the water that becomes vapor.

505 The Craig and Gordon (1969) equation models exchange with the environment, equi-
 506 librium evaporation, and turbulent and molecular diffusion. This combination of effects
 507 has a profound effect on the isotope fractionation, strongly enriching drops compared
 508 to equilibrium mixing or Rayleigh distillation.

509 We extend the work of Stewart (1975) by accounting for the drop size distribution
 510 and resolving the kinetic effects associated with diffusion in the drop-vapor laminar bound-
 511 ary layer. Assuming a spherical laminar layer around the drop, we parameterize the diameter-
 512 dependent ratio of molecular and turbulent vapor diffusion matched to previous exper-
 513 imental results. This diffusion model predicts relatively stronger molecular diffusion and
 514 kinetic enrichment for small drops. Drops become more enriched as they vanish, by 42%
 515 more than predicted by constant $n \approx 0.58$, previously measured for drops larger than
 516 1 mm diameter. Laboratory and field observations are needed to test our parameteri-
 517 zation over a wider range of drop diameters. Modeling the diffusion has several broader
 518 applications: it yields the humidity as a function of distance from an isolated drop, and
 519 it can be used to account for the effect of diffusive conduction and evaporation on drop
 520 temperature.

521 Small evaporating sea spray droplets ($D = 0.01-1.0$ mm) would be enriched by these
 522 kinetic effects. Modeling the evaporation of sea spray must also include the effect of the
 523 concentrated salt solution, which is beyond the scope of this article, but measurement
 524 of the stable isotopes in surface atmospheric water vapor, the surface ocean, and the sea
 525 spray would help constrain the rate of evaporation from the sea spray relative to evap-
 526 oration from the surface.

527 A broad range of drop sizes in the DSD further enriches the isotope ratio of the
 528 evaporated water. The precocious complete evaporation of small drops enriches δ_D
 529 of the resulting vapor by +10 ‰ compared to a single drop. Because small drops evapo-
 530 rate quickly and completely, cumulative vapor evaporated from realistic drop size dis-
 531 tributions become enriched quickly to $\delta = -20$ ‰ even with a large fraction $f \approx 0.95$ of
 532 the rain remaining.

533 The rain isotope flux divergence yields the isotope source representative of undi-
 534 luted evaporative downdraft cores. Decomposition of the deuterium rain flux divergence
 535 demonstrates that evaporation and equilibration with the surrounding vapor enriches
 536 drops, and the evaporation of these drops enriches the subcloud air deuterium by 12 ‰ per
 537 1 mm of rain accumulation. Secondly, the rain transports relatively less enriched liq-
 538 uid downward.

539 The model formulated by following the Lagrangian trajectories of drops resolved
 540 by their initial size and stable isotope ratio is conceptually and computationally expedi-
 541 ent for evaluating rain evaporation and its resulting vapor. The prediction of rain mass
 542 evaporation is more computationally expensive than the isotopes, but solutions are sim-
 543 ple nearly elliptical curves. The model can be evaluated for over large steps, or at high
 544 resolution, enabling computation of sources of stable isotopes by the rain, which can be
 545 used interpret observations and models of rain, evaporated water vapor, and their sta-
 546 ble water isotopes.

Appendix A The laminar length scale l_ν

In a laminar layer of thickness l_ν the rare water vapor isotopologue diffuses slower than the abundant vapor. Beyond this laminar layer, eddy diffusivity dominates, which diffuses both isotopologues equally. We parameterize the laminar layer thickness as

$$l_\nu = \nu/U$$

with kinematic viscosity ν and velocity scale U .

The velocity scale U is the speed of the drop relative to the surrounding air. U is usually found from the fall velocity of the drop. Small droplets (Reynolds number $Re = DU/\nu < 1$) fall with the weak velocity Stokes solution. Turbulent air velocities also accelerate the droplets, resulting in relative velocities.

We first neglect gravity and consider a velocity component of the droplet u suspended in air with velocity u_{air} . The relative speed in this component is $u' = u_{air} - u$. The inertia of the drop is balanced by the drag by the surrounding air:

$$m \frac{du}{dt} = \frac{\pi}{6} \hat{\rho}_l D^3 \frac{du}{dt} = \frac{\pi}{8} \hat{\rho} D^2 C_D (u_{air} - u) |u_{air} - u|$$

so

$$\frac{du}{dt} = \frac{3}{4} \frac{\hat{\rho}}{\hat{\rho}_l} \frac{C_D}{D} (u_{air} - u) |u_{air} - u|$$

Multiplying the equation of motion by the relative velocity u' , we write the eddy kinetic energy $u'^2/2$ equation. Neglecting correlations between anomalies u and u_{air} ,

$$\frac{d}{dt} \frac{u'^2}{2} = -k |u'^3| = -k |\overline{u_{air}^3} - \overline{u^3}|$$

with

$$k = \frac{3}{4} \frac{\hat{\rho}}{\hat{\rho}_l} \frac{C_D}{D}.$$

Though the turbulence can drive temporary velocity anomalies, mean relative velocity kinetic energy strictly dissipates by drag. Its decay rate goes to zero when the third moments of air and drop velocity balance: $\overline{u_{air}^3} = \overline{u^3}$. Though the third moments are not equivalent to second moments, we assume the third moments are equal when the variances are equal $\overline{u_{air}^2} = \overline{u^2}$.

The turbulent kinetic energy TKE is proportional to any one component of the air velocity,

$$\overline{u_{air}^2} = 2\text{TKE}/3.$$

The air and drop velocities are uncorrelated so

$$\overline{u'^2} = \overline{(u - u_{air})^2} = \overline{u^2} + \overline{u_{air}^2} = 2\overline{u_{air}^2} = 4\text{TKE}/3.$$

All three components of the velocity are geometrically orthogonal, and the mean fall velocity U_{fall} is statistically orthogonal, so their magnitudes add in quadrature,

$$U = (4\text{TKE} + U_{\text{fall}}^2)^{1/2}. \quad (\text{A1})$$

This drop-relative velocity is used for calculation of the laminar length scale. The contribution of the TKE is small, compared to the fall velocity.

Appendix B Temperature and humidity of the drop and environment

B1 Saturation deficit

Drops nearly approach the wet bulb temperature (Stewart, 1975) in an environment of uniform specific humidity q and adiabatic temperature. We first rewrite 1 by

579 noting the kinematic vapor diffusivity in air is $K_{va} = k_{va}/\hat{\rho}$ and $\Delta\hat{\rho}_v/\hat{\rho} = \Delta q = q_s(T_r) -$
 580 q_a so

$$\frac{dD}{dz} = \frac{4f_v k_{va}}{DU_{\text{fall}}\hat{\rho}_l} \Delta q.$$

581 We linearize the local saturation specific humidity $q_s(T_r)$ of the drop about a represen-
 582 tative temperature \tilde{T} . The humidity of the air $q_a = q_s(T_0)$ is saturated at the cloud
 583 base at temperature T_0 . The linearization for Δq about \tilde{T} is

$$\Delta q = q_s(T_r) - q_a = \left(\frac{\partial q_s}{\partial T} \right)_{\tilde{T}} (T_r - \tilde{T}) - q_a.$$

584 The drop temperature is very near the wet bulb temperature of the environment, yield-
 585 ing

$$\Delta q = \left(\frac{\partial q_s}{\partial T} \right)_{\tilde{T}} \Gamma_w (z' - \tau_w U_{\text{fall}})$$

586 where $z' = z_0 - z > 0$ is the displacement fallen from cloud base, and

$$\Gamma_w = \Gamma_{\text{ad}} (1 + L(\partial q_s/\partial T)_{\tilde{T}}/c_p)^{-1}$$

587 is the linearized lapse rate of wet bulb potential temperature. The adiabatic lapse rate
 588 is $\Gamma_{\text{ad}} = g/c_p$. This approximates the linear profile of RH used by Sarkar et al. (2023).
 589 The heat transport length scale $\lambda = \tau_w U_{\text{fall}}$ is the small downward displacement of cooler
 590 wet bulb temperature by the falling drop. It is largest (32 m) for the largest drops at
 591 cloud base (Appendix B), which is considerably smaller than turbulent displacements.
 592 The turbulence and the small heat transport displacement shall be neglected for con-
 593 venience.

594 B2 Drop temperature

595 A falling drop evolves toward a wet bulb temperature. Its temperature equation
 596 is

$$\frac{dT}{dt} = -\frac{12f_T K_{Ta} \hat{\rho} c_p}{D^2 \hat{\rho}_l c_w} \left[(T - T_a) + \frac{L}{c_p} \frac{f_v K_{va}}{f_h K_{Ta}} (q_s(T) - q_a) \right], \quad (\text{B1})$$

597 with kinematic conductivity $K_{Ta} = k_{Ta}/(\hat{\rho} c_p)$, vapor diffusivity in air K_{va} [$\text{m}^2 \text{s}^{-1}$],
 598 density $\hat{\rho}_l$ and specific heat of liquid water c_w , drop diameter D , and specific humidity
 599 $q = \hat{\rho}_v/\hat{\rho}$. Solution and surface tension effects are important for very small droplets and
 600 concentrated solutions (e.g., haze and sea spray; Andreas, 1995), but these effects are
 601 neglected here. Radiative heating is also neglected. For typical temperature and pres-
 602 sure below the cloud, $K_{va}/K_{Ta} = 1.16$.

603 The conventional wet bulb temperature T_{w0} is defined by $c_p(T_{w0} - T_a) = -L(q_s(T_{w0}) -$
 604 $q_a)$ but inspection of equation B1 shows that the equilibrium wet bulb temperature of
 605 a drop is slightly modified by the ratios, of vapor to temperature, of ventilation factors
 606 and diffusivities,

$$T_w = T_a - (L/c_p)(f_v K_{va}/f_h K_{Ta})(q_s(T_w) - q_a). \quad (\text{B2})$$

607 It still depends mostly on the environment T_a, q_a , and slightly on the diameter through
 608 the ventilation factors. The ratio of the ventilation factors f_v/f_h is nearly unity (Abra-
 609 ham, 1962). This effect is parameterized in the body of the paper by $n = \rho_m/rho$. The
 610 diffusivity ratio $K_{va}/K_{Ta} = 1.16$ results in a 6% increase of the air-drop temperature
 611 difference $T_a - T_w$ compared to $T_a - T_{w0}$.

612 The wet bulb temperature is practical to measure, yet it cannot be found analyt-
 613 ically from air temperature and humidity because the empirical equilibrium humidity
 614 ($q_s(T)$) cannot be inverted analytically. Corpart et al. (2023) solve for the drop temper-
 615 ature by approximating the equilibrium humidity by a quadratic. Calculating the deriva-
 616 tive $\partial q_s/\partial T$ by automatic differentiation, we solve equation B2 numerically within 10^{-3}
 617 K in two iterations of Newton's method.

618 How fast does the drop approach T_w ? The time scale for temperature conduction
619 is

$$\tau_T = \left(\frac{12f_h K_{Ta} \hat{\rho} c_p}{D^2 \hat{\rho}_l c_w} \right)^{-1}.$$

620 The wet bulb adjustment is faster because of the evaporative heating term. Linearizing
621 the saturation specific humidity about the wet bulb temperature, T_w , $q - q_s(T_w) = (\partial q_s / \partial T)_{T_w} (T -$
622 $T_w)$, we find the temperature equation adjusts as,

$$\frac{dT}{dt} = -(T - T_w)(1 + \beta) / \tau_T = -(T - T_w) / \tau_w$$

623 with

$$\beta = \frac{L}{c_p} \frac{f_v K_{va}}{f_T K_{Ta}} \left(\frac{\partial q_s}{\partial T} \right)_{T_w} \approx \frac{L}{c_p} \left(\frac{\partial q_s}{\partial T} \right)_{T_w}.$$

624 The conductive-evaporative temperature adjustment timescale for the drop is

$$\tau_w = \tau_T / (1 + \beta), \tag{B3}$$

625 which is $(1 + \beta) \sim 2.8$ times shorter than τ_T at $T = 290$ K. This timescale will be used
626 to compute the distance drops fall as their temperature adjusts.

627 Fall transport

628 Drops are cooler than the local wet bulb temperature of their environment, because
629 they fall from the cooler environment aloft. In the drop's frame of reference, T_w of the
630 environment warms as the drop descends

$$\left(\frac{dT_w}{dt} \right)_{\text{fall}} = +U_{\text{fall}} \Gamma_w$$

631 with lapse rate $\Gamma_w = dT_w / dz < 0$ and downward velocity $U_{\text{fall}} = -dz / dt > 0$. The
632 equilibrium depression from the wet bulb temperature $\Delta T = T - T_w$ is solved by bal-
633 ancing this falling source and the evaporative-conductive temperature source above:

$$0 = \frac{d}{dt} \Delta T = \left(\frac{d}{dt} \Delta T \right)_{\text{evap-cdct}} + \left(\frac{d}{dt} \Delta T \right)_{\text{fall}} = -\Delta T / \tau_w + U_{\text{fall}} \Gamma_w.$$

634 The drop temperature T is cooler than the surrounding wet bulb temperature T_w be-
635 cause the drop T adjusts to the environmental T_w over an integral length scale $\lambda = \tau_w U_{\text{fall}}$,
636 and

$$T = T_w + \lambda \Gamma_w.$$

637 The adjustment length scale λ is largest for large drops, reaching 30 m for drops $D >$
638 1 mm. This diagnoses a 1.0 mm drop has temperature $T = T_w - 0.2$ K and 0.1 mm
639 drop has $T = T_w - 0.001$ K. The difference $T - T_w$ is also small in numerical integra-
640 tions of B1. The adjustment length scale has been neglected in calculations in the body
641 of this paper.

642 Open Research

643 The NOAA PSL surface meteorology data (NOAA Physical Sciences Laboratory,
644 2020), the water isotope analyzer data (Bailey and Noone, 2021), and the rainwater iso-
645 tope analysis data (Quiñones Meléndez et al., 2022) from the *Ronald H. Brown* and EUREC4A-
646 ATOMIC field experiment are accessible from their respective references. Computational
647 notebooks written in the Julia language (Bezanson et al., 2017) are publicly archived (de
648 Szoek, 2024).

649 Acknowledgments

650 This work was supported by NSF award number 1937780 and NOAA award number NA19OAR4310375
651 (SPD, DN), and ONR award number N000142212042 (SPD). This material is based upon
652 work supported by the National Science Foundation under Grant No. AGS-1938108 (PNB).

653

References

- 654 Abraham, F. F. (1962). Evaporation of raindrops. *Journal of Geophysical*
655 *Research (1896-1977)*, 67(12), 4673–4682. Retrieved 2024-01-23, from
656 <https://onlinelibrary.wiley.com/doi/abs/10.1029/JZ067i012p04673>
657 (_eprint: <https://onlinelibrary.wiley.com/doi/pdf/10.1029/JZ067i012p04673>)
658 doi: 10.1029/JZ067i012p04673
- 659 Abraham, F. F., Jordan, S. K., Kortzeborn, R. N., & Kolsky, H. G. (1972,
660 March). Model for Time-dependent Raindrop Size Distributions; Ap-
661 plication to the Washout of Airborne Contaminants. *IBM Journal of*
662 *Research and Development*, 16(2), 91–100. Retrieved 2024-01-23, from
663 <https://ieeexplore.ieee.org/document/5391467?denied=> (Conference
664 Name: IBM Journal of Research and Development) doi: 10.1147/rd.162.0091
- 665 Andreas, E. L. (1995, April). The Temperature of Evaporating Sea Spray Droplets.
666 *Journal of the Atmospheric Sciences*, 52(7), 852–862. Retrieved 2023-10-
667 30, from [https://journals.ametsoc.org/view/journals/atsc/52/7/
668 1520-0469_1995_052_0852_ttoess_2_0_co_2.xml](https://journals.ametsoc.org/view/journals/atsc/52/7/1520-0469_1995_052_0852_ttoess_2_0_co_2.xml) (Publisher: American
669 Meteorological Society Section: Journal of the Atmospheric Sciences) doi:
670 10.1175/1520-0469(1995)052<0852:TTOESS>2.0.CO;2
- 671 Bailey, A., Aemisegger, F., Villiger, L., Los, S. A., Reverdin, G., Quiñones Meléndez,
672 E., ... Thompson, E. J. (2023, January). Isotopic measurements in wa-
673 ter vapor, precipitation, and seawater during EUREC⁴A. *Earth Sys-*
674 *tem Science Data*, 15(1), 465–495. Retrieved 2024-02-07, from [https://
675 essd.copernicus.org/articles/15/465/2023/](https://essd.copernicus.org/articles/15/465/2023/) (Publisher: Copernicus
676 GmbH) doi: 10.5194/essd-15-465-2023
- 677 Bailey, A., & Noone, D. (2021). *ATOMIC ship water vapor isotopic analyzer:*
678 *Near-surface humidity and water vapor isotope ratios from an isotopic an-*
679 *alyzer aboard NOAA Ship Ronald H. Brown in the North Atlantic Ocean,*
680 *near Barbados: Atlantic Tradewind Ocean-Atmosphere Mesoscale Interaction*
681 *Campaign 2010-01-26 to 2020-02-10 (NCEI Accession 0225417).* NOAA
682 National Centers for Environmental Information. Retrieved 2024-02-20,
683 from <https://doi.org/10.25921/s76r-1n85>. (ItemType: dataset) doi:
684 10.25921/s76r-1n85
- 685 Best, A. C. (1952). The evaporation of raindrops. *Quarterly Journal of the*
686 *Royal Meteorological Society*, 78(336), 200–225. Retrieved 2024-01-22, from
687 <https://onlinelibrary.wiley.com/doi/abs/10.1002/qj.49707833608>
688 (_eprint: <https://onlinelibrary.wiley.com/doi/pdf/10.1002/qj.49707833608>) doi:
689 10.1002/qj.49707833608
- 690 Bezanson, J., Edelman, A., Karpinski, S., & Shah, V. B. (2017, January). Julia: A
691 Fresh Approach to Numerical Computing. *SIAM Review*, 59(1), 65–98. Re-
692 trieved 2024-02-20, from <https://epubs.siam.org/doi/10.1137/141000671>
693 (Publisher: Society for Industrial and Applied Mathematics) doi: 10.1137/
694 141000671
- 695 Brutsaert, W. (1965). A model for evaporation as a molecular diffusion
696 process into a turbulent atmosphere. *Journal of Geophysical Research*
697 *(1896-1977)*, 70(20), 5017–5024. Retrieved 2024-02-20, from [https://
698 onlinelibrary.wiley.com/doi/abs/10.1029/JZ070i020p05017](https://onlinelibrary.wiley.com/doi/abs/10.1029/JZ070i020p05017) (_eprint:
699 <https://onlinelibrary.wiley.com/doi/pdf/10.1029/JZ070i020p05017>) doi:
700 10.1029/JZ070i020p05017
- 701 Brutsaert, W. (1975, October). The Roughness Length for Water Vapor Sensi-
702 ble Heat, and Other Scalars. *Journal of the Atmospheric Sciences*, 32(10),
703 2028–2031. Retrieved 2020-08-21, from [https://journals.ametsoc.org/
704 jas/article/32/10/2028/18389/The-Roughness-Length-for-Water
705 -Vapor-Sensible-Heat](https://journals.ametsoc.org/jas/article/32/10/2028/18389/The-Roughness-Length-for-Water-Vapor-Sensible-Heat) (Publisher: American Meteorological Society) doi:
706 10.1175/1520-0469(1975)032<2029:TRLFVW>2.0.CO;2
- 707 Corpart, M., Restagno, F., & Boulogne, F. (2023, October). Analytical prediction

- 708 of the temperature and the lifetime of an evaporating spherical droplet. *Col-*
 709 *loids and Surfaces A: Physicochemical and Engineering Aspects*, 675, 132059.
 710 Retrieved 2024-01-22, from [https://www.sciencedirect.com/science/](https://www.sciencedirect.com/science/article/pii/S0927775723011433)
 711 [article/pii/S0927775723011433](https://www.sciencedirect.com/science/article/pii/S0927775723011433) doi: 10.1016/j.colsurfa.2023.132059
- 712 Craig, H., & Gordon, L. I. (1965). Deuterium and oxygen 18 variations in the ocean
 713 and the marine atmosphere. In Tongiorgi, E. (Ed.), *Stable Isotopes in Oceanographic Studies and Palaeotemperatures* (pp. 9–130). Pisa: Lab. Geologia Nu-
 714 cleare.
 715
- 716 Crawford, J., Hollins, S. E., Meredith, K. T., & Hughes, C. E. (2017). Precip-
 717 itation stable isotope variability and subcloud evaporation processes in a
 718 semi-arid region. *Hydrological Processes*, 31(1), 20–34. Retrieved 2024-02-
 719 25, from <https://onlinelibrary.wiley.com/doi/abs/10.1002/hyp.10885>
 720 (_eprint: <https://onlinelibrary.wiley.com/doi/pdf/10.1002/hyp.10885>) doi:
 721 10.1002/hyp.10885
- 722 Dansgaard, W. (1964, November). Stable isotopes in precipitation. *Tellus*, 16(4),
 723 436–468. Retrieved 2022-04-08, from [http://tellusa.net/index.php/](http://tellusa.net/index.php/tellusa/article/view/8993)
 724 [tellusa/article/view/8993](http://tellusa.net/index.php/tellusa/article/view/8993) doi: 10.1111/j.2153-3490.1964.tb00181.x
- 725 de Szoek, S. P. (2024). *Shallow cumulus rain drop evaporation and isotope model*
 726 *notebooks* [Software: Julia Jupyter computational notebooks]. Retrieved from
 727 <https://ir.library.oregonstate.edu/concern/datasets/br86bc57n>
 728 (Publisher: Oregon State University) doi: 10.7267/br86bc57n
- 729 Galewsky, J., Steen-Larsen, H. C., Field, R. D., Worden, J., Risi, C., & Schneider,
 730 M. (2016). Stable isotopes in atmospheric water vapor and applications to the
 731 hydrologic cycle. *Reviews of Geophysics*, 54(4), 809–865. Retrieved 2022-04-08,
 732 from <https://onlinelibrary.wiley.com/doi/abs/10.1002/2015RG000512>
 733 (_eprint: <https://onlinelibrary.wiley.com/doi/pdf/10.1002/2015RG000512>) doi:
 734 10.1002/2015RG000512
- 735 Garratt, J. R. (1992). *The atmospheric boundary layer*. Cambridge.
- 736 Gat, J. R. (1996). Oxygen and Hydrogen Isotopes in the Hydrologic Cycle. *An-*
 737 *nuual Review of Earth and Planetary Sciences*, 24(1), 225–262. Retrieved 2022-
 738 12-06, from <https://doi.org/10.1146/annurev.earth.24.1.225> (_eprint:
 739 <https://doi.org/10.1146/annurev.earth.24.1.225>) doi: 10.1146/annurev.earth.24
 740 .1.225
- 741 Graf, P., Wernli, H., Pfahl, S., & Sodemann, H. (2019, January). A new interpreta-
 742 tive framework for below-cloud effects on stable water isotopes in vapour and
 743 rain. *Atmospheric Chemistry and Physics*, 19(2), 747–765. Retrieved 2023-12-
 744 06, from <https://acp.copernicus.org/articles/19/747/2019/> (Publisher:
 745 Copernicus GmbH) doi: 10.5194/acp-19-747-2019
- 746 Hiron, T., & Flossmann, A. I. (2020). Oxygen Isotopic Fractionation in Clouds:
 747 A Bin-Resolved Microphysics Model Approach. *Journal of Geophysical Re-*
 748 *search: Atmospheres*, 125(21), e2019JD031753. Retrieved 2024-02-25, from
 749 <https://onlinelibrary.wiley.com/doi/abs/10.1029/2019JD031753>
 750 (_eprint: <https://onlinelibrary.wiley.com/doi/pdf/10.1029/2019JD031753>)
 751 doi: 10.1029/2019JD031753
- 752 Kinzer, G. D., & Gunn, R. (1951). The evaporation, temperature and thermal
 753 relaxation-time of freely falling waterdrops. *Journal of Meteorology*, 8(2), 71–
 754 83.
- 755 Lee, J.-E., & Fung, I. (2008). “Amount effect” of water isotopes and
 756 quantitative analysis of post-condensation processes. *Hydrologi-*
 757 *cal Processes*, 22(1), 1–8. Retrieved 2024-01-24, from [https://](https://onlinelibrary.wiley.com/doi/abs/10.1002/hyp.6637)
 758 onlinelibrary.wiley.com/doi/abs/10.1002/hyp.6637 (_eprint:
 759 <https://onlinelibrary.wiley.com/doi/pdf/10.1002/hyp.6637>) doi: 10.1002/
 760 hyp.6637
- 761 Li, X., & Srivastava, R. C. (2001, September). An Analytical Solution for Raindrop
 762 Evaporation and Its Application to Radar Rainfall Measurements. *Journal*

- 763 of *Applied Meteorology and Climatology*, 40(9), 1607–1616. Retrieved 2024-
 764 01-22, from [https://journals.ametsoc.org/view/journals/apme/40/9/
 765 1520-0450_2001_040_1607_aasfre_2.0.co_2.xml](https://journals.ametsoc.org/view/journals/apme/40/9/1520-0450_2001_040_1607_aasfre_2.0.co_2.xml) (Publisher: American Me-
 766 teorological Society Section: Journal of Applied Meteorology and Climatology)
 767 doi: 10.1175/1520-0450(2001)040(1607:AASFRE)2.0.CO;2
- 768 Merlivat, L. (1978). Molecular diffusivities of H₂¹⁶O, HD¹⁶O, and H₂¹⁸O in gases.
 769 *The Journal of Chemical Physics*, 69(6), 2864–2871. Retrieved 2021-02-23,
 770 from <https://aip.scitation.org/doi/abs/10.1063/1.436884> (Publisher:
 771 American Institute of Physics) doi: 10.1063/1.436884
- 772 Merlivat, L., & Jouzel, J. (1979, January). Global climatic interpretation of the
 773 deuterium-oxygen 18 relationship for precipitation. *Journal of Geophysical Re-
 774 search*, 84, 5029–5033. doi: 10.1029/JC084iC08p05029
- 775 NOAA Physical Sciences Laboratory. (2020). *The Atlantic Tradewind Ocean-
 776 Atmosphere Mesoscale Interaction Campaign (ATOMIC), Barbados, Jan 17
 777 - Feb 12, 2020. Ronald H. Brown Meteorology and Navigation.* NOAA Na-
 778 tional Centers for Environmental Information. Retrieved from [https://
 779 www.ncei.noaa.gov/archive/accession/ATOMIC-2020](https://www.ncei.noaa.gov/archive/accession/ATOMIC-2020)
- 780 Noone, D. (2012). Pairing Measurements of the Water Vapor Isotope Ratio with
 781 Humidity to Deduce Atmospheric Moistening and Dehydration in the Tropi-
 782 cal Midtroposphere. *Journal of Climate*, 25(13), 4476–4494. Retrieved from
 783 <http://journals.ametsoc.org/doi/abs/10.1175/JCLI-D-11-00582.1> doi:
 784 10.1175/JCLI-D-11-00582.1
- 785 Noone, D., & Simmonds, I. (2002). Associations between δ18O of Water
 786 and Climate Parameters in a Simulation of Atmospheric Circulation for
 787 1979–95. *Journal of Climate*, 15(22), 3150–3169. Retrieved 2024-02-
 788 29, from [https://journals.ametsoc.org/view/journals/clim/15/22/
 789 1520-0442_2002_015_3150_aboowa_2.0.co_2.xml](https://journals.ametsoc.org/view/journals/clim/15/22/1520-0442_2002_015_3150_aboowa_2.0.co_2.xml) (Publisher: Ameri-
 790 can Meteorological Society Section: Journal of Climate) doi: 10.1175/
 791 1520-0442(2002)015(3150:ABOOWA)2.0.CO;2
- 792 Quinn, P. K., Thompson, E. J., Coffman, D. J., Baidar, S., Bariteau, L., Bates,
 793 T. S., ... Zuidema, P. (2021, April). Measurements from the RV *Ronald
 794 H. Brown* and related platforms as part of the Atlantic Tradewind Ocean-
 795 Atmosphere Mesoscale Interaction Campaign (ATOMIC). *Earth System
 796 Science Data*, 13(4), 1759–1790. Retrieved 2023-10-19, from [https://
 797 essd.copernicus.org/articles/13/1759/2021/](https://essd.copernicus.org/articles/13/1759/2021/) (Publisher: Copernicus
 798 GmbH) doi: 10.5194/essd-13-1759-2021
- 799 Quiñones Meléndez, E., de Szoeki, S. P., & David, N. (2022). *ATOMIC ship
 800 rain sampler : Rainwater isotope ratios from samples taken aboard NOAA
 801 Ship Ronald H. Brown in the North Atlantic Ocean, near Barbados: Atlantic
 802 Tradewind Ocean-Atmosphere Mesoscale Interaction Campaign 2020-01-05 to
 803 2020-02-11 (NCEI Accession 0244402).* NOAA National Centers for Envi-
 804 ronmental Information. Retrieved 2024-02-20, from [https://www.ncei.noaa.
 805 gov/access/metadata/landing-page/bin/iso?id=gov.noaa.nodc:0244402](https://www.ncei.noaa.gov/access/metadata/landing-page/bin/iso?id=gov.noaa.nodc:0244402)
 806 (Last Modified: 2024-02-17) doi: 10.25921/bbje-6y41
- 807 Risi, C., Muller, C., & Blossey, P. (2021). Rain Evaporation, Snow Melt,
 808 and Entrainment at the Heart of Water Vapor Isotopic Variations in
 809 the Tropical Troposphere, According to Large-Eddy Simulations and
 810 a Two-Column Model. *Journal of Advances in Modeling Earth Sys-
 811 tems*, 13(4), e2020MS002381. Retrieved 2024-02-20, from [https://
 812 onlinelibrary.wiley.com/doi/abs/10.1029/2020MS002381](https://onlinelibrary.wiley.com/doi/abs/10.1029/2020MS002381) (_eprint:
 813 <https://onlinelibrary.wiley.com/doi/pdf/10.1029/2020MS002381>) doi:
 814 10.1029/2020MS002381
- 815 Salamalikis, V., Argiriou, A. A., & Dotsika, E. (2016, February). Isotopic mod-
 816 eling of the sub-cloud evaporation effect in precipitation. *Science of The
 817 Total Environment*, 544, 1059–1072. Retrieved 2023-06-15, from <https://>

- 818 www.sciencedirect.com/science/article/pii/S0048969715310536 doi:
819 10.1016/j.scitotenv.2015.11.072
- 820 Sarkar, M., Bailey, A., Blossey, P., de Szoeko, S. P., Noone, D., Quiñones Meléndez,
821 E., ... Chuang, P. Y. (2023, October). Sub-cloud rain evaporation in
822 the North Atlantic winter trade winds derived by pairing isotopic data
823 with a bin-resolved microphysical model. *Atmospheric Chemistry and
824 Physics*, 23(19), 12671–12690. Retrieved 2023-12-05, from [https://
825 acp.copernicus.org/articles/23/12671/2023/](https://acp.copernicus.org/articles/23/12671/2023/) (Publisher: Copernicus
826 GmbH) doi: 10.5194/acp-23-12671-2023
- 827 Sengupta, S., Bhattacharya, S. K., Sunil, N. S., & Sonar, S. (2023, July). Quan-
828 tifying Raindrop Evaporation Deficit in General Circulation Models from
829 Observed and Model Rain Isotope Ratios on the West Coast of India. *At-
830 mosphere*, 14(7), 1147. Retrieved 2024-02-20, from [https://www.mdpi.com/
831 2073-4433/14/7/1147](https://www.mdpi.com/2073-4433/14/7/1147) (Number: 7 Publisher: Multidisciplinary Digital
832 Publishing Institute) doi: 10.3390/atmos14071147
- 833 Stevens, B., Bony, S., Farrell, D., Ament, F., Blyth, A., Fairall, C., ... Zöger, M.
834 (2021, August). EUREC⁴A. *Earth System Science Data*, 13(8), 4067–4119.
835 Retrieved 2023-11-16, from [https://essd.copernicus.org/articles/13/
836 4067/2021/](https://essd.copernicus.org/articles/13/4067/2021/) (Publisher: Copernicus GmbH) doi: 10.5194/essd-13-4067-2021
- 837 Stewart, M. K. (1975). Stable isotope fractionation due to evaporation and
838 isotopic exchange of falling waterdrops: Applications to atmospheric
839 processes and evaporation of lakes. *Journal of Geophysical Research
840 (1896-1977)*, 80(9), 1133–1146. Retrieved 2023-02-03, from [https://
841 onlinelibrary.wiley.com/doi/abs/10.1029/JC080i009p01133](https://onlinelibrary.wiley.com/doi/abs/10.1029/JC080i009p01133) (eprint:
842 <https://onlinelibrary.wiley.com/doi/pdf/10.1029/JC080i009p01133>) doi:
843 10.1029/JC080i009p01133
- 844 Thurnherr, I., Kozachek, A., Graf, P., Weng, Y., Bolshiyarov, D., Landwehr, S., ...
845 Aemisegger, F. (2020, May). Meridional and vertical variations of the water
846 vapour isotopic composition in the marine boundary layer over the Atlantic
847 and Southern Ocean. *Atmospheric Chemistry and Physics*, 20(9), 5811–5835.
848 Retrieved 2024-02-25, from [https://acp.copernicus.org/articles/20/
849 5811/2020/](https://acp.copernicus.org/articles/20/5811/2020/) (Publisher: Copernicus GmbH) doi: 10.5194/acp-20-5811-2020
- 850 Tremoy, G., Vimeux, F., Soumana, S., Souley, I., Risi, C., Favreau, G., & Oï,
851 M. (2014). Clustering mesoscale convective systems with laser-based wa-
852 ter vapor $\delta^{18}\text{O}$ monitoring in Niamey (Niger). *Journal of Geophysical
853 Research: Atmospheres*, 119(9), 5079–5103. Retrieved 2024-02-25, from
854 <https://onlinelibrary.wiley.com/doi/abs/10.1002/2013JD020968>
855 (eprint: <https://onlinelibrary.wiley.com/doi/pdf/10.1002/2013JD020968>)
856 doi: 10.1002/2013JD020968

Figure 1.

ship observations of a cold pool

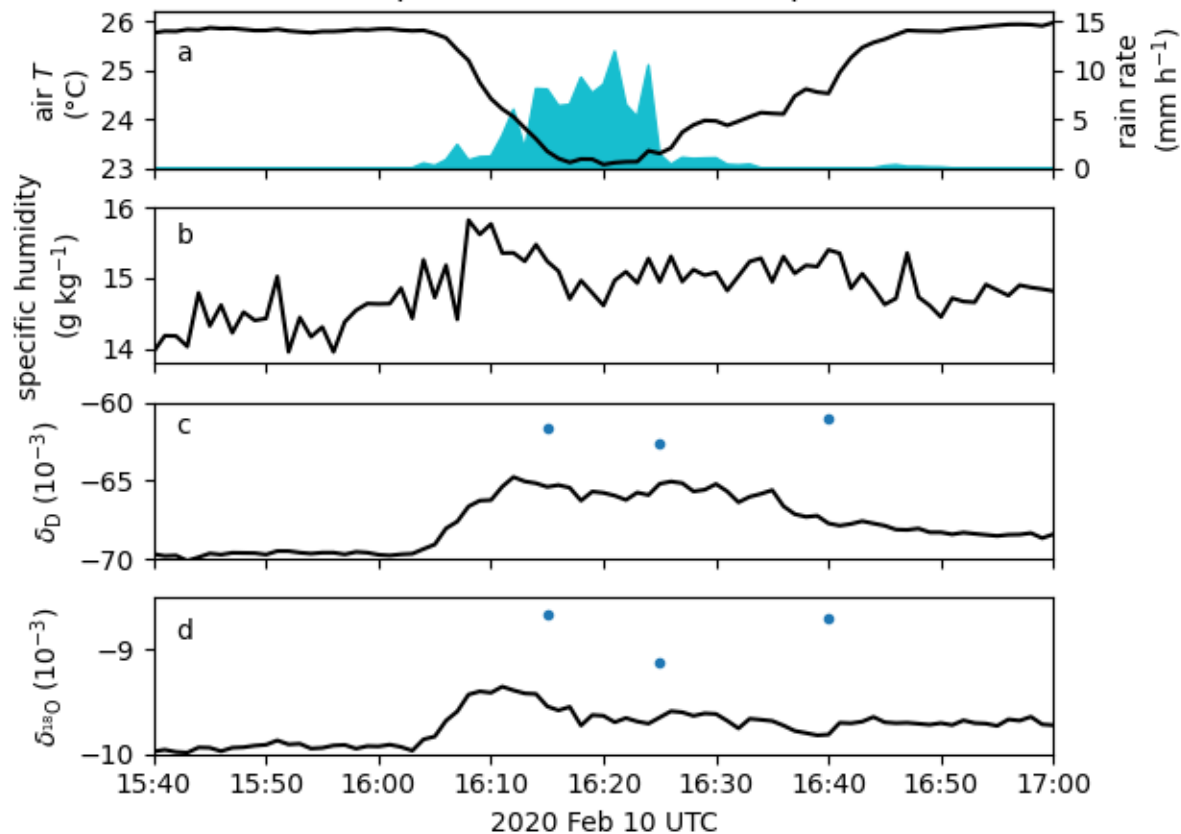


Figure 2.

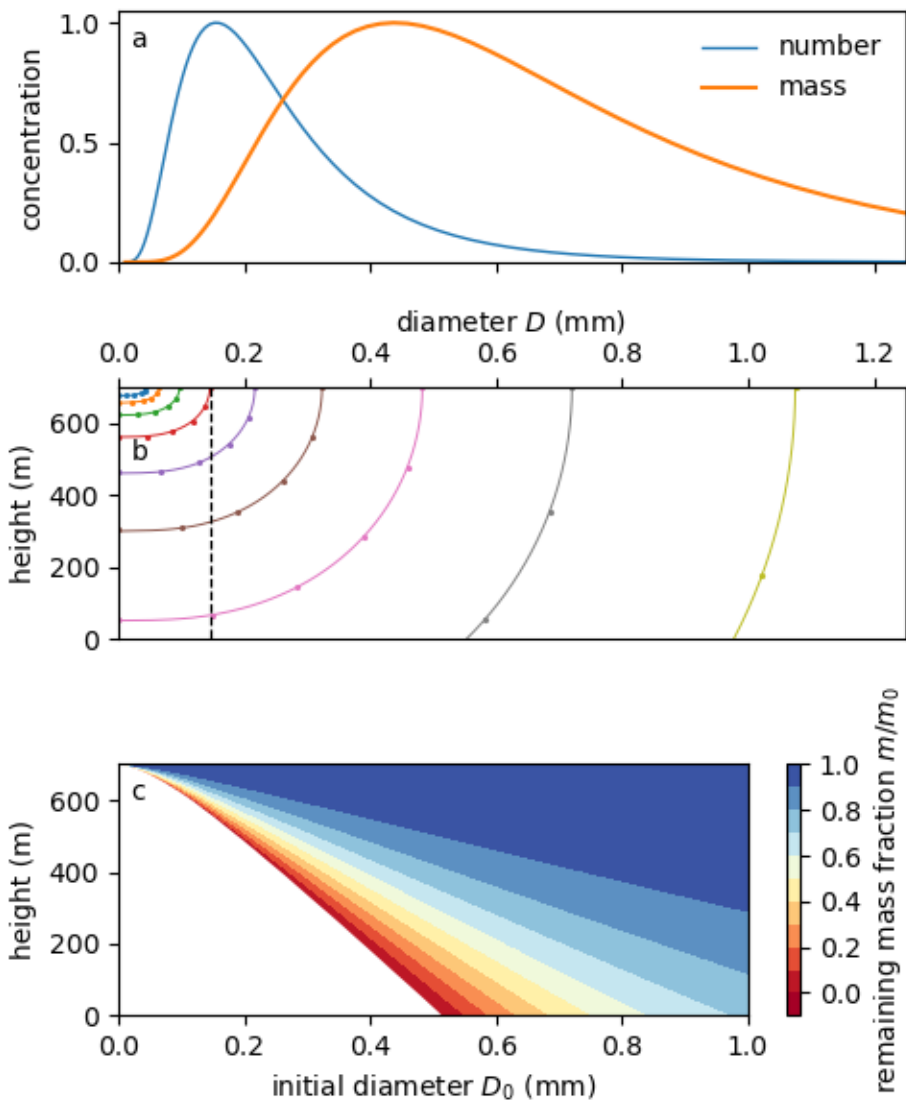


Figure 3.

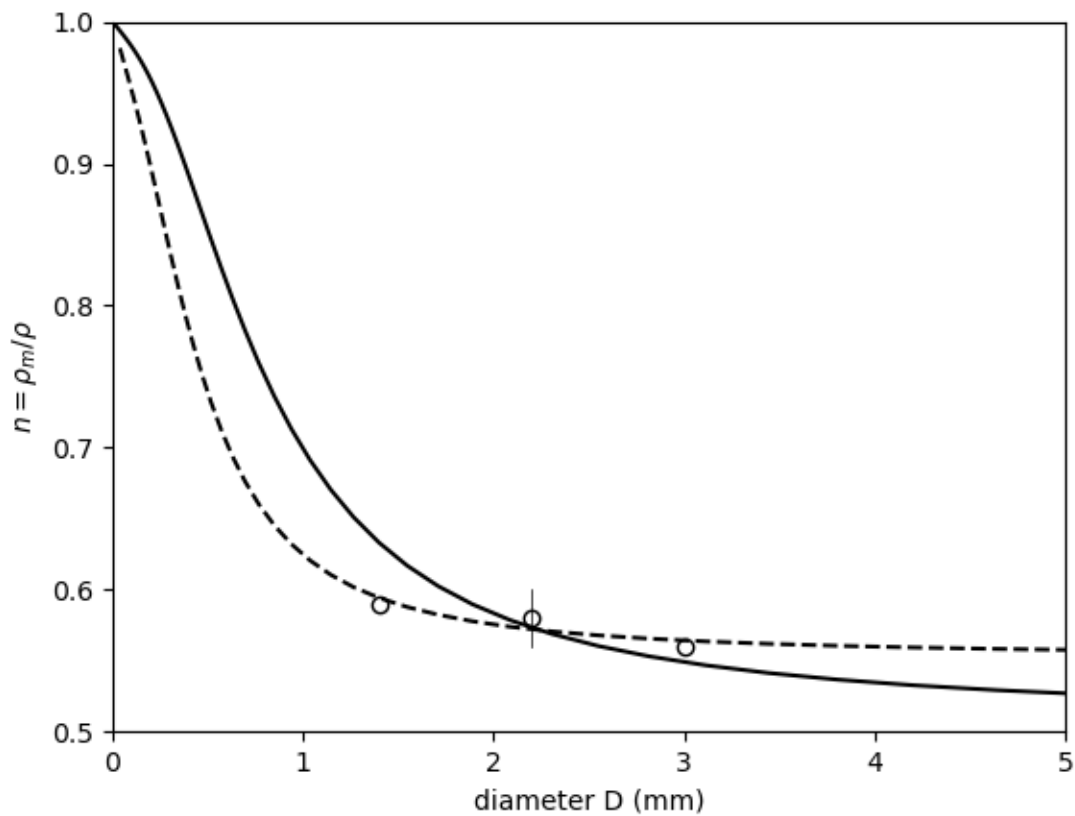


Figure 4.

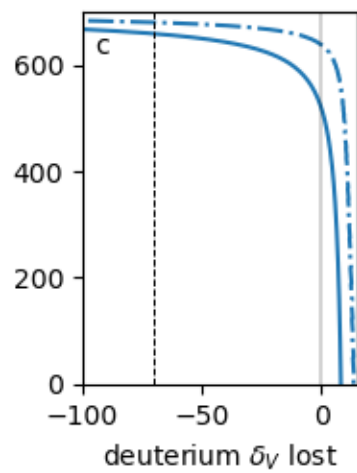
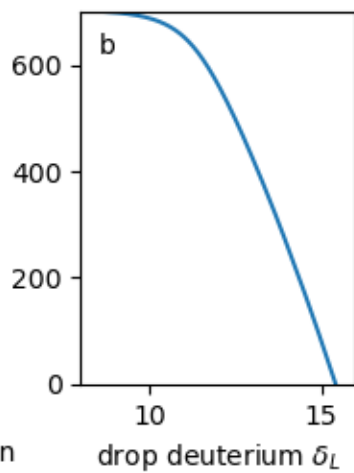
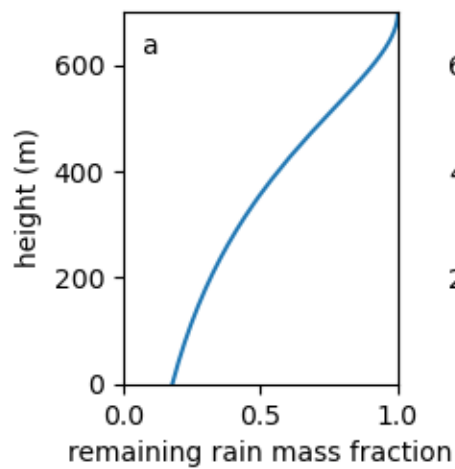
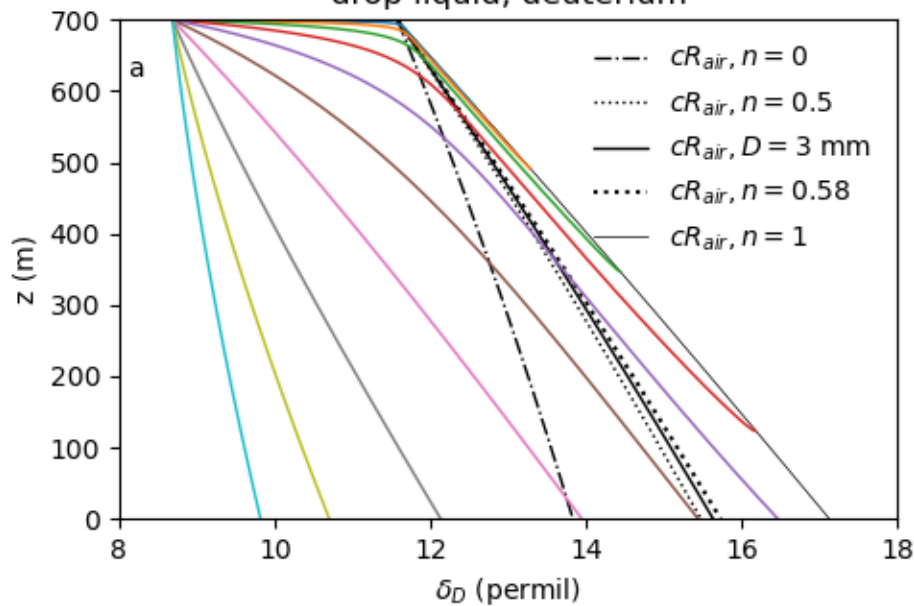


Figure 5.

drop liquid, deuterium



drop liquid, oxygen-18

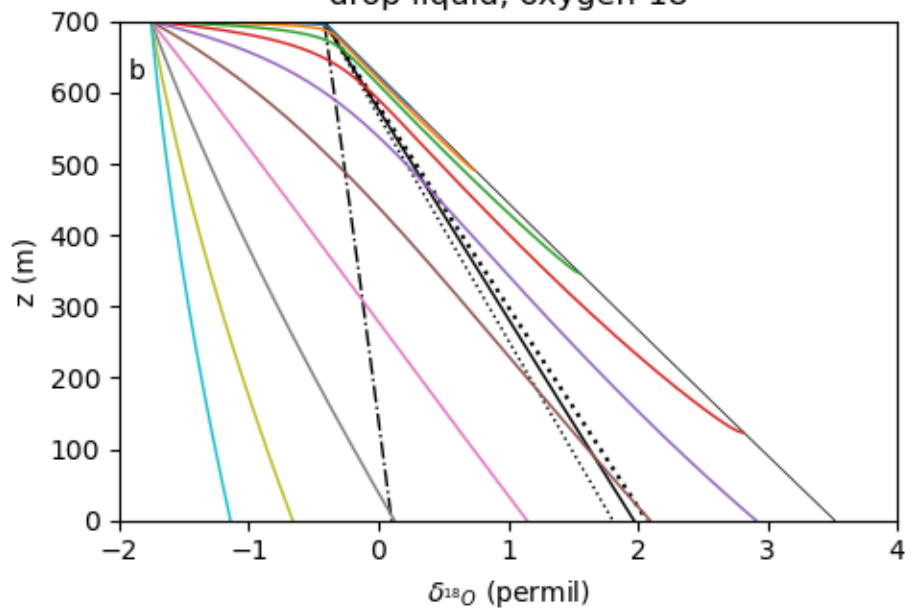


Figure 6.

liquid

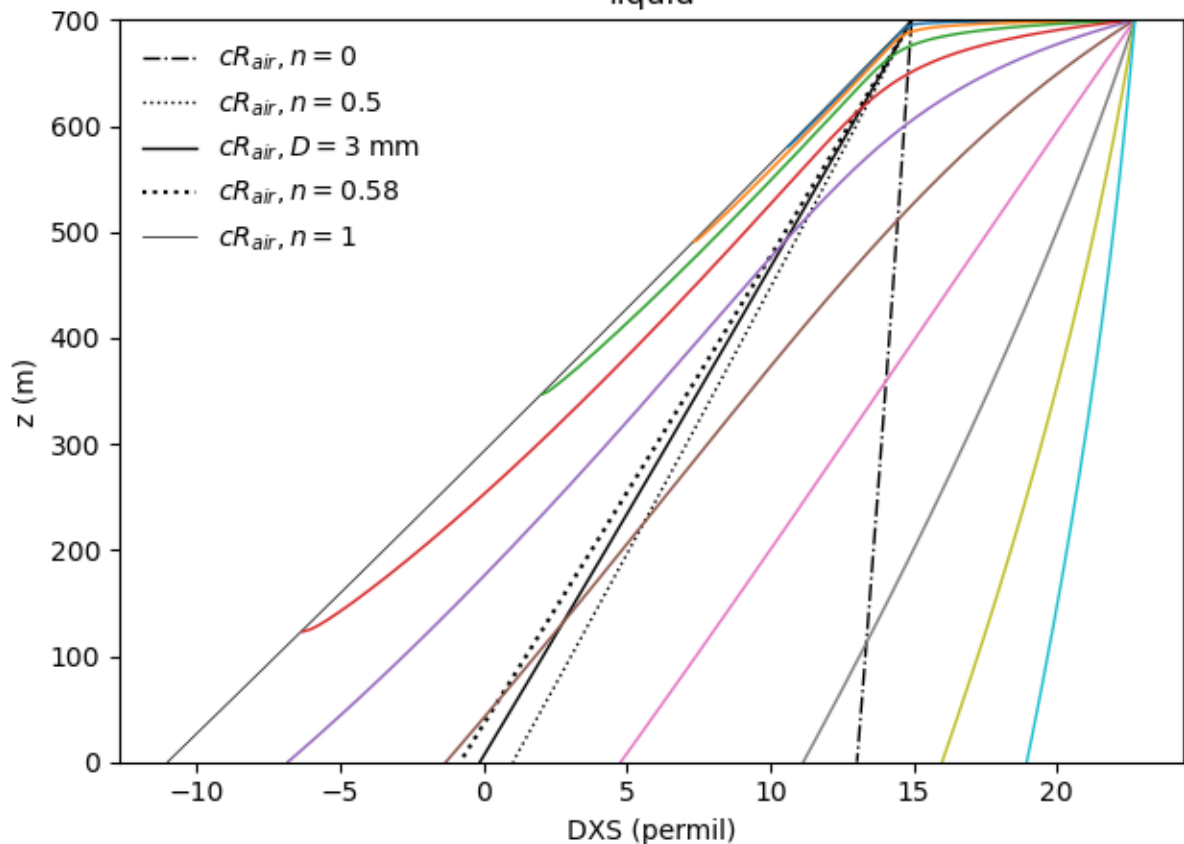


Figure 7.

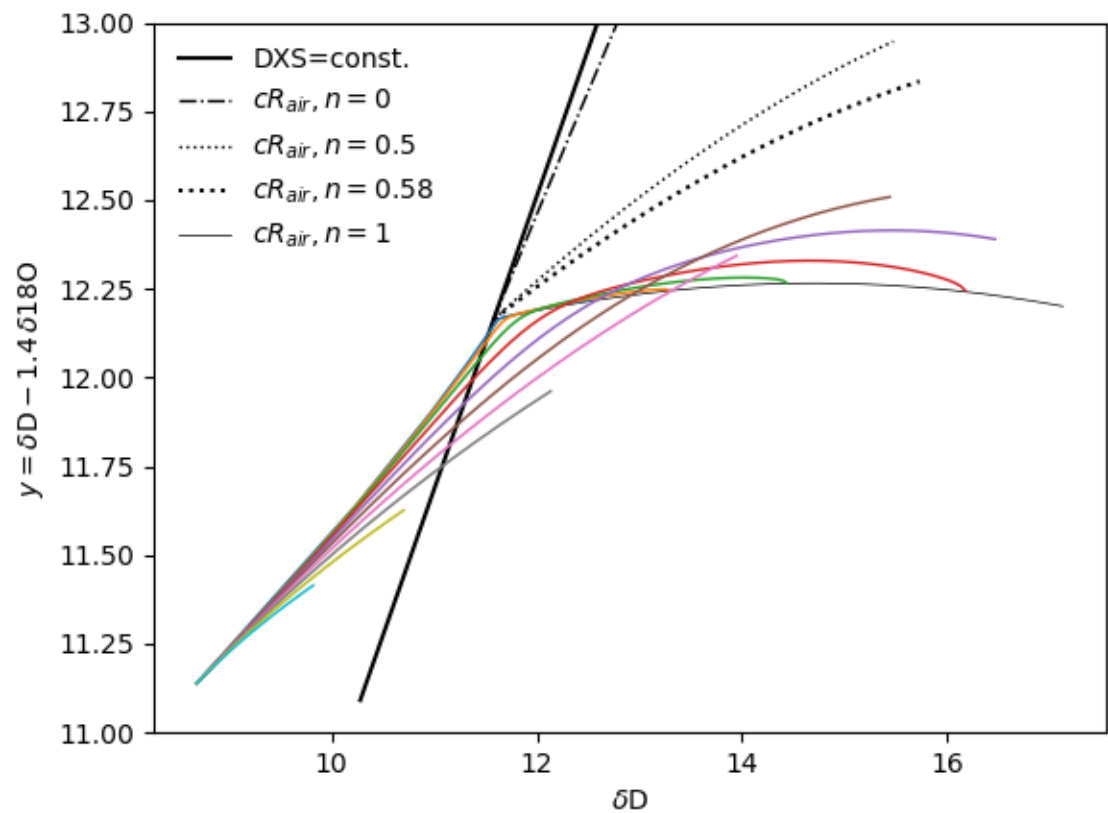


Figure 8.

vapor lost from drops

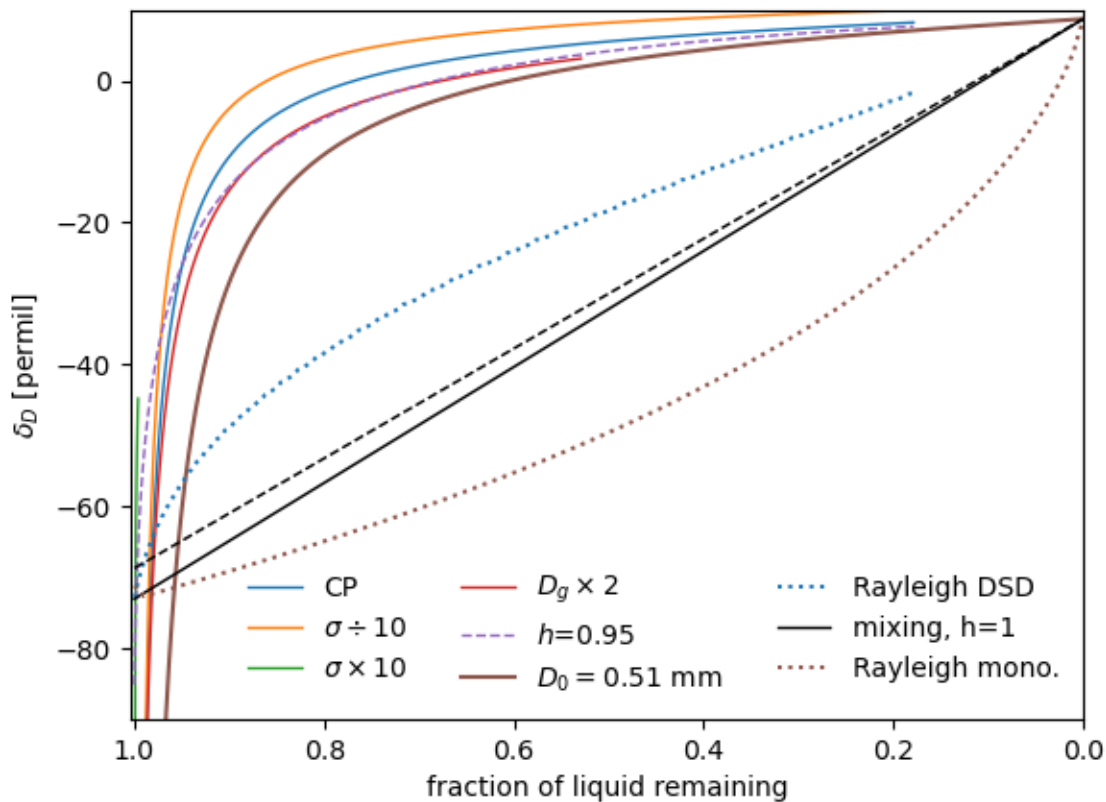


Figure 9.

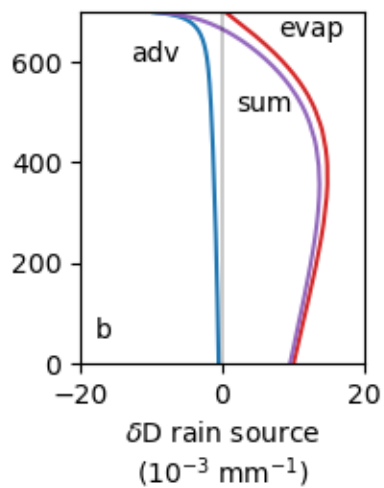
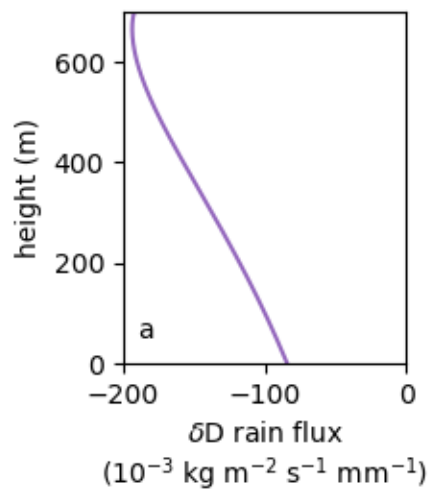


Figure 10.

liquid equilibrium experiments, $\delta_{L0} = \delta_{air} = 0$

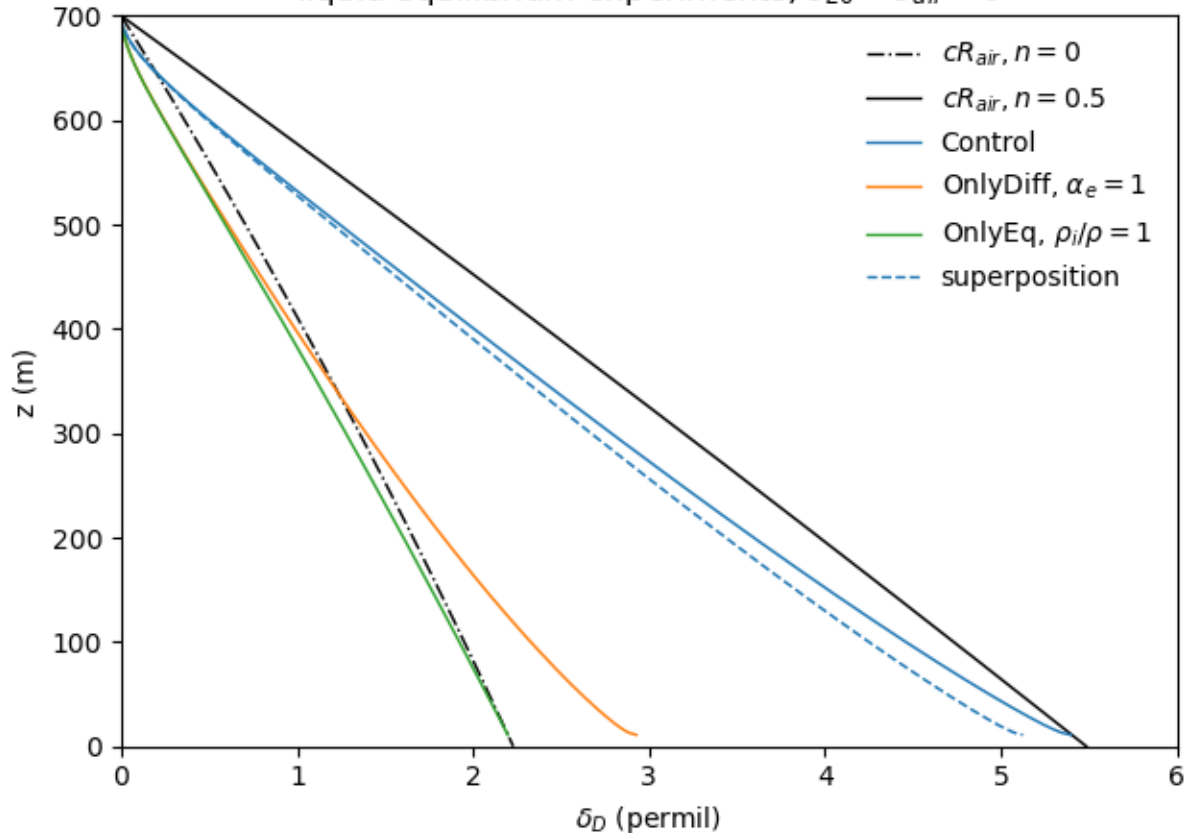


Figure 11.

liquid enriched experiments, $\delta_{L0} = 0$, $\delta_{air} = -1$

